Gastroenterology 2022;162:590–603

BASIC AND TRANSLATIONAL—PANCREAS

Activating Immune Recognition in Pancreatic Ductal Adenocarcinoma via Autophagy Inhibition, MEK Blockade, and CD40 Agonism

Honglin Jiang,[1,5] Tristan Courau,[2,3] Joseph Borison,[4] Alexa J. Ritchie,[1,5] Aaron T. Mayer,[4] Matthew F. Krummel,[2,3,5] and Eric A. Collisson[1,5]

[1]Division of Hematology and Oncology, Department of Medicine, University of California San Francisco, San Francisco, California; [2]Department of Pathology, University of California San Francisco, San Francisco, California; [3]ImmunoX Initiative, University of California San Francisco, San Francisco, California; [4]Enable Medicine, Menlo Park, California; and [5]Helen Diller Family Comprehensive Cancer Center, University of California San Francisco, San Francisco, California

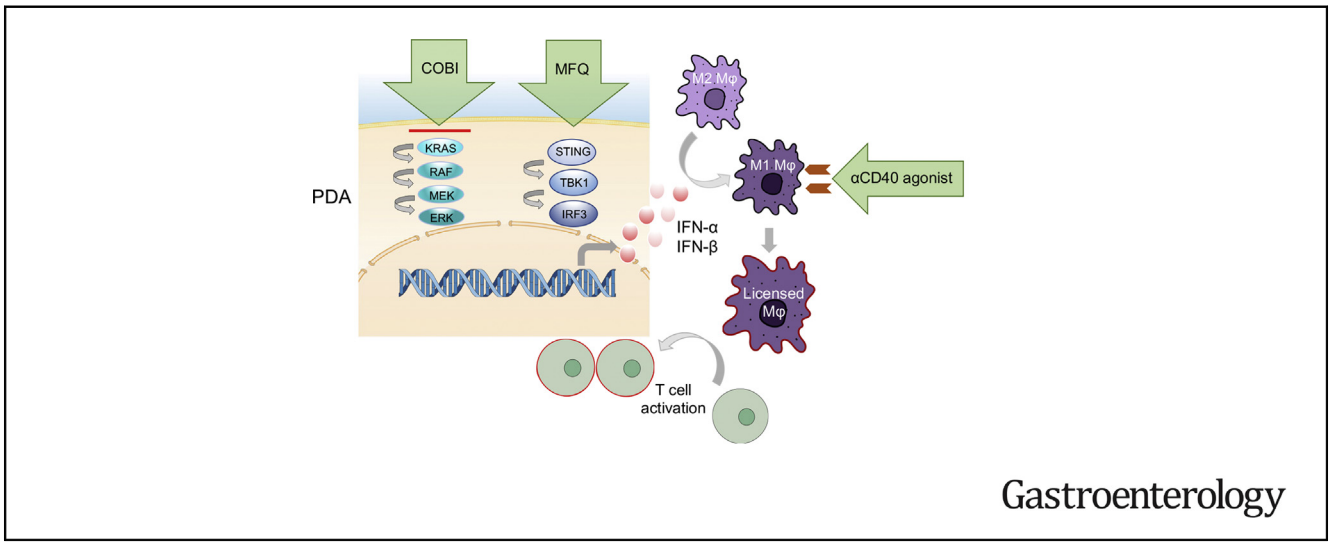

See Covering the Cover synopsis on page 358.

BACKGROUND AND AIMS: Patients with pancreatic ductal adenocarcinoma (PDA) have not yet benefitted from the revolution in cancer immunotherapy due in large part to a dominantly immunosuppressive tumor microenvironment. MEK inhibition combined with autophagy inhibition leads to transient tumor responses in some patients with PDA. We examined the functional effects of combined MEK and autophagy inhibition on the PDA immune microenvironment and the synergy of combined inhibition of MEK and autophagy with CD40 agonism (aCD40) against PDA using immunocompetent model systems. **METHODS:** We implanted immunologically "cold" murine PDA cells orthotopically in wide type C57BL/6J mice. We administered combinations of inhibitors of MEK1/2, inhibitors of autophagy, and aCD40 and measured anticancer efficacy and immune sequelae using mass cytometry and multiplexed immunofluorescence imaging analysis to characterize the tumor microenvironment. We also used human and mouse PDA cell lines and human macrophages in vitro to perform functional assays to elucidate the cellular effects induced by the treatments. **RESULTS:** We find that coinhibition of MEK (using cobimetinib) and autophagy (using mefloquine), but not either treatment alone, activates the STING/type I interferon pathway in tumor cells that in turn activates paracrine tumor associated macrophages toward an immunogenic M1-like phenotype. This switch is further augmented by aCD40. Triple therapy (cobimetinib + mefloquine + aCD40) achieved cytotoxic T-cell activation in an immunologically "cold" mouse PDA model, leading to enhanced antitumor immunity. **CONCLUSIONS:** MEK and autophagy coinhibition coupled with aCD40 invokes immune repolarization and is an attractive therapeutic approach for PDA immunotherapy development.

Keywords: Pancreatic Ductal Adenocarcinoma; Autophagy; CD40 Agonism; MAPK Pathway; Macrophage Polarization.

Abbreviations used in this paper: **aCD40, CD40 agonism; APCs, antigen-presenting cells; BafA1, bafilomycin A1; CAFs, cancer-associated fibroblasts; cDC2, type-2 conventional dendritic cells; cGAS, cyclic GMP–AMP synthase; COBI, cobimetinib; CODEX, co-detection by indexing; cyTOF, cytometry by time of flight; GFP, green fluorescent protein; HCQ, hydroxychloroquine; iCAF, inflammatory cancer-associated fibroblasts; IFN, interferon; IRF, interferon regulatory factors; mAb, monoclonal antibody; MFQ, mefloquine; NK, natural killer; PBS, phosphate-buffered saline; PDA, pancreatic ductal adenocarcinoma; STING, stimulator of interferon genes; TAMs, tumor-associated macrophages.**

Most current article

0016-5085/$36.00
https://doi.org/10.1053/j.gastro.2021.09.066

Pancreatic ductal adenocarcinoma (PDA) is a leading cause of cancer death in the United States.[1] Immunotherapies that have revolutionized the care of many other cancers have had no meaningful impact on PDA and long-term survival remains low.[2] *KRAS* mutations drive >90% of human PDAs.[3] Mutant Ras proteins signal largely down the RAF/MEK/MAPK pathway in PDA,[4] but inhibition of this pathway with potent inhibitors of MEK1/2 is compensated for by increases in autophagocytic flux. Inhibiting lysosomal acidification with hydroxychloroquine therapeutically synergizes with MEK or ERK inhibition[5,6] and is currently under clinical investigation (NCT03825289). The combination of MEK inhibition with autophagy inhibition is thought to operate by a tumor cell-autonomous mechanism, without any specific requirement for immunocompetency per se.

Immune reactivation as a strategy to fight pancreatic cancer has been largely unsuccessful to date. Blockade of PD-1/PD-L1, either alone or with CTLA-4 coblockade,[7] or with chemotherapy[8] were not effective outside of the extremely rare microsatellite-unstable setting[9] indicating potent immune evasion by PDA cells, a dominant acting immunosuppressive microenvironment,[10] or both.

We sought to explore the functional effects of combined MEK and autophagy inhibition on the PDA immune microenvironment through the study of multiple immune-competent, preclinical model systems. We found that coinhibition of MEK and autophagy led to transcriptional activation of inflammatory cytokines in the cancer cell. These signals affect macrophages' polarization to favor a M1-like, antigen-presenting phenotype. This effect was mediated in part by STING, was further augmented by CD40 agonism (aCD40), and led to T-cell–dependent tumor killing in vivo, prolonging overall survival in immunocompetent mouse models of the disease.

WHAT YOU NEED TO KNOW

BACKGROUND AND CONTEXT

Immune reactivation as a strategy to fight pancreatic ductal adenocarcinoma (PDA) has been largely unsuccessful to date due in large part to a dominantly immunosuppressive tumor microenvironment.

NEW FINDINGS

We discovered that coinhibition of MEK and autophagy led to a STING/type I interferon pathway in tumor cells. This effect was further augmented by CD40 agonism, and led to T-cell–dependent tumor killing in vivo, prolonging overall survival in immunocompetent mouse models of the disease.

LIMITATIONS

Mouse models do not entirely mimic PDA progression in humans, and more work is needed using human model systems.

IMPACT

MEK and autophagy coinhibition coupled with CD40 agonism augments antitumor immunity and is an attractive therapeutic approach for PDA immunotherapy development.

Materials and Methods

The detailed methodology is described in the Supplementary Materials and Methods.

Cell Lines

MiaPaca-2, HPAF II, HPAC, and Panc 02.03 are from American Type Culture Collection. 6694C2 cells were kindly provided by Dr Ben Stanger and FC1245 cells were kindly provided by Dr David Tuveson. Cells were maintained at 37°C in a humidified incubator at 5% CO_2. Cells were grown in appropriate media as recommended by American Type Culture Collection, and supplemented with 10% fetal bovine serum (Gibco, Waltham, MA) and 1% penicillin/streptomycin (Gibco). All cell lines tested were negative for mycoplasma contamination.

Animals and In Vivo Procedures

C57BL/6J mice were purchased from Jackson Laboratory. $P48^{Cre}$; $Kras^{LSL\text{-}G12D/+}$; $Trp53^{flox/flox}$ (KPC) mouse was a gift of Matthias Hebrok (University of California, San Francisco). All animal experiments were conducted in the American Association for Accreditation of Laboratory Animal Care-accredited University of California, San Francisco in accordance with all applicable local requirements, including approval by the Institutional Animal Care and Use Committee. For orthotopic pancreas implantation, 6- to 7-week-old mice were administered intrapancreatic injections of 6694C2 (provided by Dr Ben Stanger) or FC1245 (provided by Dr David Tuveson) PDA cells derived from KPC mice. Cells were transduced in vitro with a lentiviral vector (pCDH, Addgene 72265) encoding a firefly luciferase. Cells were suspended in phosphate-buffered saline (PBS) with 50% Matrigel (BD Biosciences) and 5×10^5 cells for 6694C2-fLuc and 1000 cells for FC1245-fLuc tumor cells were injected into the body of the pancreas via laparotomy. Bioluminescent imaging (Xenogen IVIS) was performed 2–3 times a week to monitor tumor growth. Mice were euthanized ~3 weeks later and tumors were harvested for analyses. Alternatively, mice bearing parental 6694C2 tumors or p48cre-driven PDA mice were monitored using ultrasound (Vevo 2100) and analyzed in tumor progression and survival experiments.

Mass Cytometry

Mass cytometry (CyTOF) was performed as described elsewhere.[11] Briefly, conjugations of mass cytometry antibodies with metal isotopes were done using the Maxpar conjugation kit (Fluidigm) according to the manufacturer's protocols and each antibody was titrated to define its optimal staining concentration. After labeling, antibodies were diluted in Candor PBS Antibody Stabilization solution (Candor Bioscience) supplemented with 0.02% NaN3 to 0.2 mg/mL and stored long term at 4°C. Each sample, initially stained with cisplatinium, fixed with 3.2% paraformaldehyde, and frozen at -80C on day of harvesting, was thawed and barcoded by mass-tag labelling with distinct combinations of stable Pd isotopes in 0.02% saponin in PBS before further pooling and staining. For staining, cells were first resuspended in cell-staining media (Fluidigm) containing metal-labeled antibodies against CD16/32 for 5 minutes at room temperature to block Fc receptors, followed by

the addition of a cocktail containing surface marker antibodies in a final volume of 500 μL for 30 minutes at room temperature. Cells were then permeabilized with methanol for 10 minutes at 4°C, washed, and incubated with a cocktail containing intracellular marker antibodies in a final volume of 500 μL for 30 minutes at room temperature. Cells were finally stained with 191/193Ir DNA intercalator (Fluidigm) diluted in PBS with 1.6% paraformaldehyde 48 hours before data acquisition. For acquisition, cells were washed and resuspended at 1 mol/L/mL in deionized water + 10% EQ four element calibration beads (Fluidigm) and run on a CyTOF mass cytometer (Fluidigm). We acquired an average of 1–3 $\times$ 10^5 cells per sample, consistent with generally accepted practices in the field. After data collection, we used the Premessa pipeline (https://github.com/ParkerICI/premessa) to normalize data and deconvolute individual samples. We then manually gated the individual flow cytometry standard files using FlowJo (BD) according to the gating scheme described in the Supplementary Materials and Methods. In parallel, we performed unsupervised clustering analyses of either total CD45+ cells or total T cells, extracted from the manual gating strategy, using the R package Phenograph.[12] Heatmaps presented from these analyses were created using the Morpheus tool (Broad Institute). The antibodies used in our CyTOF panel are listed in the Supplementary Materials and Methods.

CODEX Multiplexed Imaging Analysis

A 23-plex custom CODEX mouse panel was developed and validated (Enable Medicine) using purified, carrier-free antibodies conjugated to unique DNA oligonucleotides. CODEX staining and imaging was performed on pancreatic mouse tumors using this panel following the manufacturer's protocol (Akoya Bioscience). Raw fluorescent TIFF image files were processed, deconvolved, and background subtracted, and antibody staining was visually assessed for each biomarker and tissue region using the ImageJ software (Fiji, version 2.0.0). TIFF hyper stacks were segmented based on 4′,6-diamidino-2-phenylindole nuclear stain, pixel intensities were quantified, and spatial fluorescence compensation was performed, which generated comma-separated value and flow cytometry standard files for downstream analysis. Cell types were enumerated via manual gating (Immune Atlas) based on canonic marker expression values and were confirmed via visual overlay of the cell populations on the immunofluorescent images using the multiplex analysis viewer (Akoya Biosciences). Voronoi diagrams were created based on the spatial coordinates of the cell types and used to mathematically compute adjacent "cell-cell" contacts. Representation of the gating strategy was described in the Supplementary Materials and Methods.

Quantification and Statistical Analysis

Statistical tests were performed using GraphPad Prism 7.0. Two-sided 2-sample *t* tests were used for comparisons of the means of data between 2 groups. One-way analysis of variance was used for comparisons among multiple independent groups. Significance of overall survival was determined using Kaplan-Meier survival curve with log-rank analysis. For animal studies, animals were randomized before treatments, and all animals treated were included for the analyses.

Results

Mefloquine Compares Favorably to Hydroxychloroquine to Inhibit Autophagy In Vivo and Synergizes With MEK Inhibition in PDA

Inhibition of autophagy is an emerging strategy for pancreatic cancer, but in the clinic is currently limited by the onset of action and potency of available agents. Hydroxychloroquine (HCQ) is widely used clinically for the treatment of psoriasis but was developed as an antimalarial medication. Other antimalarial medications, namely mefloquine (MFQ), have superior pharmacokinetic properties to HCQ and may more potently inhibit autophagy in cancer cells.[13] To measure autophagy under treatment with HCQ or MFQ both with and without MEK inhibition, we used multiple assessments of autophagic flux. We first confirmed that MEK inhibition led to expected increased autophagosome assembly, in agreement with previous reports,[6] as evidenced by accumulation of LC3B in MiaPaca2 PDA cells (Figure 1*A* and *B*, Supplementary Figure 1*A*). Additional treatment with HCQ or MFQ, which inhibit acidification of the lysosome, both effectively led to a further elevated accumulation of LC3B (Figure 1*A* and *B*, Supplementary Figure 1*A*). We observed potent antiproliferative effects at MFQ concentrations of 1 μmol/L when combined with cobimetinib (COBI) at 100 nmol/L in MiaPaca2 cells (Figure 1*C*). Potent and durable autophagy inhibition is important to prevent MEK inhibitor escape in PDA, so we next tested the duration of autophagy inhibition in vivo. We implanted FC1245 mouse PDA cells stably expressing a tandem fluorescence LC3 reporter (mCherry-green fluorescent protein [GFP]-LC3)[14] orthotopically and treated tumor-bearing mice with either MFQ or HCQ (Figure 1*D*). Inhibition of lysosome by HCQ or MFQ led to the accumulation of nonacidic autolysosomes dually fluorescent for red and green LC3. A single dose of MFQ resulted in more GFP-positive tumor cells (indicating more potent deacidification of the lysosome) at 3 and as long as 5 days after treatment (Figure 1*E* and *F*). Similarly, treatment of MiaPaCa2 and PANC-1 reporter cells with either HCQ or MFQ led to the expected increase of GFP-positive cells (Supplementary Figure 1*B*). Given these results, we anchored our in vivo autophagy inhibition approaches on the MFQ backbone for the remainder of the study.

Combined MEK and Autophagy Inhibition Activates STING/type I-Interferon Pathway in PDA Cells

The cytokine secretion profile of PDA cells is driven by Kras and plays an important role in immune evasion.[15–17] To evaluate the effects of MEK and autophagy inhibition on cytokine secretion by PDA cells, we examined transcription of inflammatory cytokine genes in syngeneic PDA orthotopic tumors (FC1245) from mice treated with MFQ (M), Cobimetinib (C), or both. We harvested the tumors after treatment, sorted out tumor cells, and found that the type I interferons (IFNs) *IFN-*α/β were dramatically up-regulated under combined MEK and autophagy inhibition. Type II

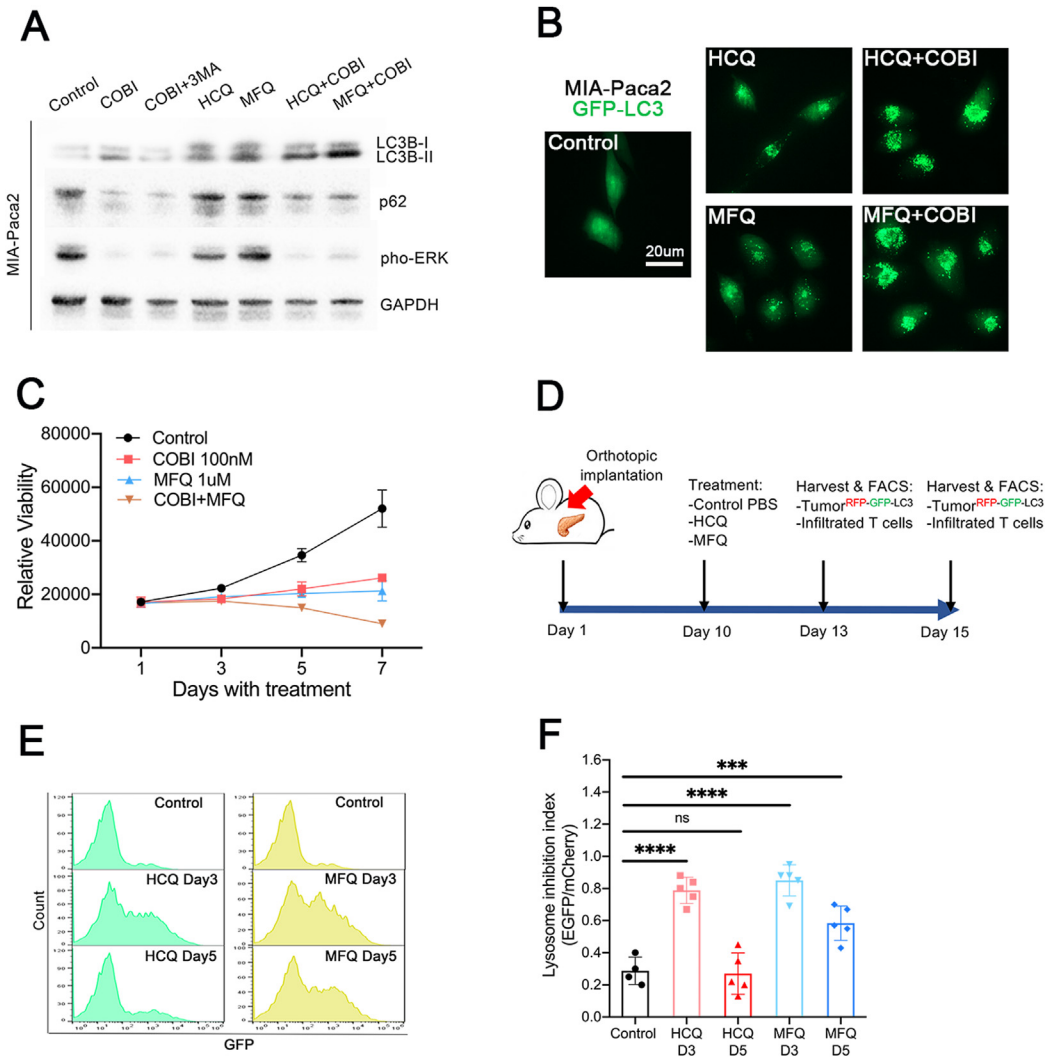

Figure 1. (*A*) Western blot for LC3B, p62, pERK, and total ERK in MiaPaca-2 cells with indicated treatment. (*B*) Representative images of LC3 expression in MiaPaca-2 cells carrying GFP-LC3 with indicated treatment. (*C*) Viability of MiaPaca-2 cells with indicated treatment. (*D*) Scheme of implantation, dose, and harvest schedule for (*E*) and (*F*). (*E*) Representative histogram assessing GFP expression of FC1245 tumors stably expressing mCherry-GFP-LC3. (*F*) Quantification of lysosome inhibition measured by the percentage of GFP/mCherry positivity. Error bars represent the mean ± SEM, n = 3 mice/group, and 1-way analysis of variance (ANOVA) was used. ***$P < .001$, ****$P < .0001$. Data were consistent across 2 independent experiments in (*C*) and (*F*).

IFNs (IFN-γ) and other cytokines examined were not induced by cotreatment (Figure 2*A*). In vitro treatment of previously described immunologically "cold" PDA cell lines (6694C2)[10] confirmed that MFQ combined with inhibition of MEK increased type I IFN transcription, lending generalization to this treatment approach in PDA (Figure 2*B*). We next used an IFN-α/β sensitive reporter cell line B16-blue[18] to quantify the amount of functional IFN protein present in the media of mouse PDA cells treated with the indicated drugs. We found that combining MEK and autophagy inhibition resulted in up-regulation of functional type I IFN proteins (Figure 2*C*). The innate immune STING-IFN pathway plays a critical role in antiviral defense and cancer. We found that autophagy inhibition by MFQ as well as vacuolar H+-ATPase inhibitor bafilomycin A1 (BafA1) in combination with COBI led to the most significant STING pathway activation as evidenced by increased expression of STING, pho-TBK1, and pho-IRF3 in human PDA cell lines MiaPaca2 and PANC10.05 (Figure 2*D*). Furthermore, immunofluorescence staining revealed a substantial fraction of the STING puncta with either MFQ or combined COBI and MFQ treatment (Figure 2*E*). In vivo treatment with either MFQ or COBI/MFQ in mouse orthotopic 6694C2 tumors induced a significant increase of STING, pho-IRF3, and STAT1 (signal transducer and activator of transcription 1) expression (Figure 2*F* and *G*, Supplementary Figure 1*C* and *D*). Similar STING-type I-IFN pathway activation was observed with in vitro treatment in a panel of human PDA cells induced, as evidenced by increased messenger RNA transcription of IFNs, STATs, and interferon regulatory factors (IRFs) (Supplementary Figure 2*A*). We hypothesized that combined MEK and autophagy inhibition led to

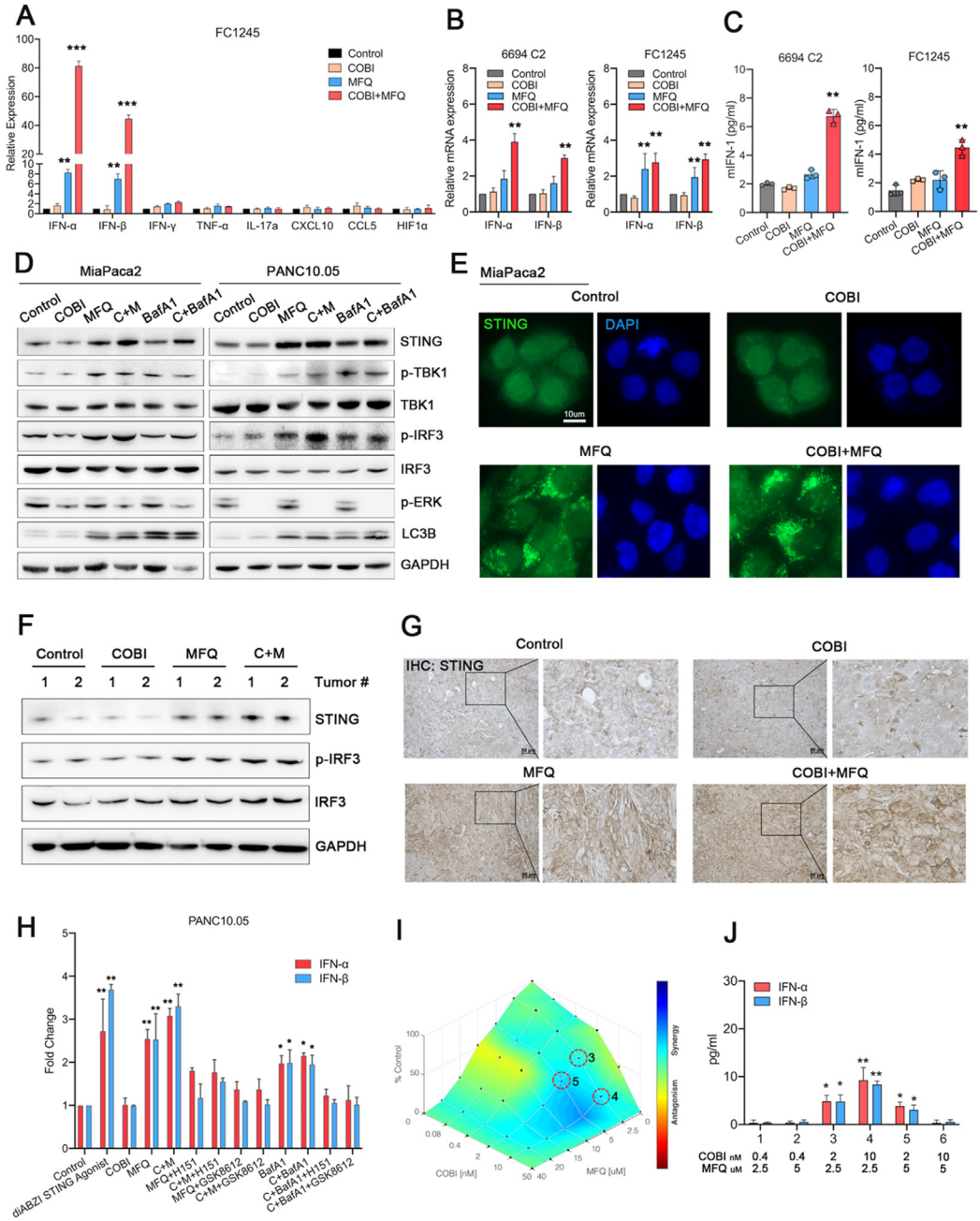

Figure 2. (*A*) Quantitative polymerase chain reaction analysis of a panel of cytokines in FC1245 tumor cells freshly isolated from FC1245 orthotopic engraftments with indicated treatment. (*B*) Quantitative polymerase chain reaction analysis of IFN α/β in 6694C2 and FC1245 cells receiving vehicle, COBI (10 nmol/L), MFQ (2.5 μmol/L), and the combination of COBI and MFQ treatment in vitro. (*C*) The amount of IFN proteins present in the media of mouse PDA cells (6694C2 and FC1245 cells) receiving vehicle, COBI (10 nmol/L), MFQ (2.5 μmol/L), and the combination of COBI and MFQ treatment quantified by IFN-α/β sensitive B16-blue reporter cell line. (*D*) Western blot for STING, p-TBK1, TBK1, pIRF3, IRF3, p-ERK, LC3B, and glyceraldehyde 3-phosphate dehydrogenase (GAPDH) expression in MiaPaca2 and PANC10.05 cells receiving vehicle, COBI (10 nmol/L), MFQ (2.5 μmol/L), BafA1 (300 nmol/L), and the combination treatments for 12 hours. (*E*) Immunofluorescence analysis for STING expression in MiaPaca2 cells receiving vehicle, COBI (10 nmol/L), MFQ (2.5 μmol/L), and the combination of COBI and MFQ treatment for 12 hours. Scale bars: 10 μm. (*F*) Western blot for STING, pIRF3, IRF3 and GAPDH in whole 6694C2 tumor lysates after indicated treatments. (*G*) Immunohistochemistry for orthotopic 6694C2 engraftments stained with STING with indicated treatment. Scale bars: 50 μm. (*H*) Enzyme-linked immunoassay (ELISA) analysis for IFN-α/β production in PANC10.05 cells with indicated treatments for 18 hours. Doses for the treatments were COBI of 10 nmol/L, MFQ of 2.5 μmol/L, diABZI of 150 nmol/L, GSK8612 of 1 μmol/L, H151 of 0.5 μmol/L, and BafA1 of 300 nmol/L. (*I*) 6694C2 cells were treated for 48 hours as indicated with cobimetinib and MFQ and analyzed for cell viability. Synergy graphs were generated using Combenefit Software. *Red circles* indicate the dose combinations in (*J*). (*J*) 6694C2 cells treated with the combination of cobimetinib and MFQ and IFN-α/β production measure using ELISA assay. Error bars represent mean ± SEM. Data were consistent across 2 independent experiments in (*A*), (*B*), (*C*), (*H*), (*I*), and (*J*). Significance determined using 1-way ANOVA and shown as **P* < .05, ***P* < .01, and ****P* < .001.

increased production of type I IFN by activating the STING pathway. In this framework, inhibition of the STING pathway should block the effects of COBI/MFQ on IFN production. To test this, a palette of pharmacologic agonist of STING (diABZI) and inhibitors of STING (H151) and TBK1 (GSK8612) was used in MiaPaca2 and PANC10.05 cells. We found that STING agonist (diABZI) alone induced a significant increase of IFN-α/β production as expected. Inhibition of STING by H151 and TBK1 by GSK8612 could effectively reduce IFN-α/β production followed by MFQ or COBI/MFQ treatment (Figure 2*H*, Supplementary Figure 2*B*). Consistently, H151 and GSK8612 effectively abrogated the ability of BafA1 or COBI/BafA1 to increase IFN-α/β expression in human PDA cells (Figure 2*H*, Supplementary Figure 2*B*). We next treated 6694C2 PDA cells with different concentrations of COBI or MFQ, either alone or in combination, and assessed drug synergy/antagonism using the Loewe Additivity method (Figure 2*I*).[19] We observed synergistic antiproliferative effects of MFQ and MEK combinations at MFQ concentrations in the 5–15 μmol/L range when combined with COBI in the range of 10–50 nmol/L (Figure 2*I*). Interestingly, lower drug levels were needed to increase production of type I IFNs compared with those required for cytostatic/cidal in vitro, indicating that lower, more clinically tolerable doses might be sufficient to elicit this in vivo effect (Figure 2*J*). We conclude from these experiments that combined MEK and autophagy inhibition cooperate to activate STING/type I IFN pathway in PDA cancer cells at doses below those required for their cytostatic/cidal effects.

CD40 Agonist Synergizes With COBI/MFQ to Inhibit PDA Progression

Type I IFNs directly or indirectly influence multiple immune cell types, including monocytes, antigen-presenting cells (APCs), natural killer (NK) cells, and lymphocytes.[20–22] Certain tumor-associated macrophages (TAMs) and certain populations of dendritic cells both serve as APCs and promote cytotoxic T-cell recruitment in the tumor microenvironment. These APCs can become fully "licensed" after CD40 ligand engagement.[23] As such, we hypothesized that the doublet of COBI/MFQ might functionally synergize with CD40 activation to improve the control of tumor outgrowth in an IFN-1 and T-cell–dependent manner.

To explore the therapeutic potential of adding activating CD40 ligand to the doublet regimen, we implanted C57BL/6J mice with syngeneic, immunologically "cold" 6694C2 cells[10] orthotopically, in the pancreas. We began treatment 5 days later with low doses of COBI plus MFQ followed by aCD40 monoclonal antibody (mAb) in an intermittent dosing schedule as shown in Figure 3*A*. Tumor growth was significantly decreased in COBI/MFQ/aCD40-treated mice compared with either COBI/MFQ or aCD40 mAb monotreated mice (Figure 3*B* and *C*, Supplementary Figure 2*C*). In addition, long-term treatment of established 6694C2 tumors (non-fLuc labeled) on day 10 with COBI/MFQ/aCD40 caused significant regression and enhanced survival, including apparent cures (Figure 3*D* and *E*, Supplementary Figure 2*D*). We subsequently rechallenged mice that were cured of the primary tumor with the triplet of COBI/MFQ/aCD40 with a second implantation of 6694C2 tumor cells (this time subcutaneously) 40 days later and observed a failure of engraftment despite robust growth of the same cells implanted in treatment-naive control C57BL/6J animals (Figure 3*F*). Similar results were seen with a second syngeneic PDA cell line (FC1245) also derived from a C57BL/6J KPC mouse (Figure 3*G* and *H*). We next evaluated the efficacy of COBI/MFQ/aCD40 in a widely used autochthonous $p48^{Cre}$; $Kras^{LSL\text{-}G12D/+}$; $Trp53^{flox/flox}$ (KPC) mouse PDA model. We initiated treatment with the triplet of COBI/MFQ/aCD40 or vehicle when the tumor size reached around 1 cm measured using ultrasound. Mice receiving the triplet of COBI/MFQ/aCD40 exhibited significant tumor shrinkage and showed prolonged overall survival compared with vehicle-treated mice (Figure 3*I* and *J*).

COBI/MFQ/aCD40 Combination Therapy Triggers Immune Activation in the PDA Tumor Microenvironment

To investigate the changes in the tumor immune microenvironment induced by our treatments, we performed supervised and unsupervised analyses of mass cytometry (CyTOF) data obtained from mice bearing 6694C2 tumors and treated with either COBI/MFQ/aCD40, aCD40 alone, COBI/MFQ, or vehicle (Figure 4*A*–*C*, Supplementary Figure 3*A*–*B*). Globally, the COBI/MFQ/aCD40 regimen induced strikingly overall infiltration of $CD45^+$ cells in the tumor (Figure 4*C*, Supplementary Figure 3*B*). Unsupervised clustering of the immune cells from all groups revealed that the density of T cells increased slightly under the treatments with COBI/MFQ or aCD40 monotherapy but were dramatically elevated with the treatment of COBI/MFQ/aCD40 (Figure 4*C*, Supplementary Figure 3*B*). Furthermore, the triple therapy of COBI/MFQ/aCD40 induced a remarkable increase in the density of TAMs, type-2 conventional dendritic cells (cDC2), and NK cells (Figure 4*C*, Supplementary Figure 3*B*). Our clustering revealed 2 subpopulations of cDC2, differing by their expression of CD301b as previously described,[24] and showed that our triple therapy mostly increased the $CD301b^-$ subset of cDC2 whereas the $CD301b^+$ subset was found decreased in the conditions where aCD40 was used (Supplementary Figure 3*B*). In line with previous reports,[25] we also observed that aCD40, alone or in combination, induced a moderate loss of type-1 conventional dendritic cells (cDC1) in the tumor (Supplementary Figure 3*B*). Interestingly, aCD40 alone was sufficient to induce a shift by decreasing protumorigenic populations of granulocytes such as $Ly6G+Siglec\text{-}F^{hi}$ neutrophils[26] and eosinophils (Supplementary Figure 3*B*). We also observed that the expression of CD16/32, CD11b, and major histocompatibility complex class II (MHCII) significantly increased on NK cells, in agreement with earlier reports that the STING-IFNs pathway can prime strong effector activity in NK cells[27] (Supplementary Figure 3*C*).

We then performed unsupervised clustering of T cells alone to define the particular subsets affected by the treatments (Figure 4*D*–*F*, Supplementary Figure 3*D*). This showed that COBI/MFQ or aCD40 alone induced a slight increase in both CD4 Teff and CD8 T-cell density, and that a

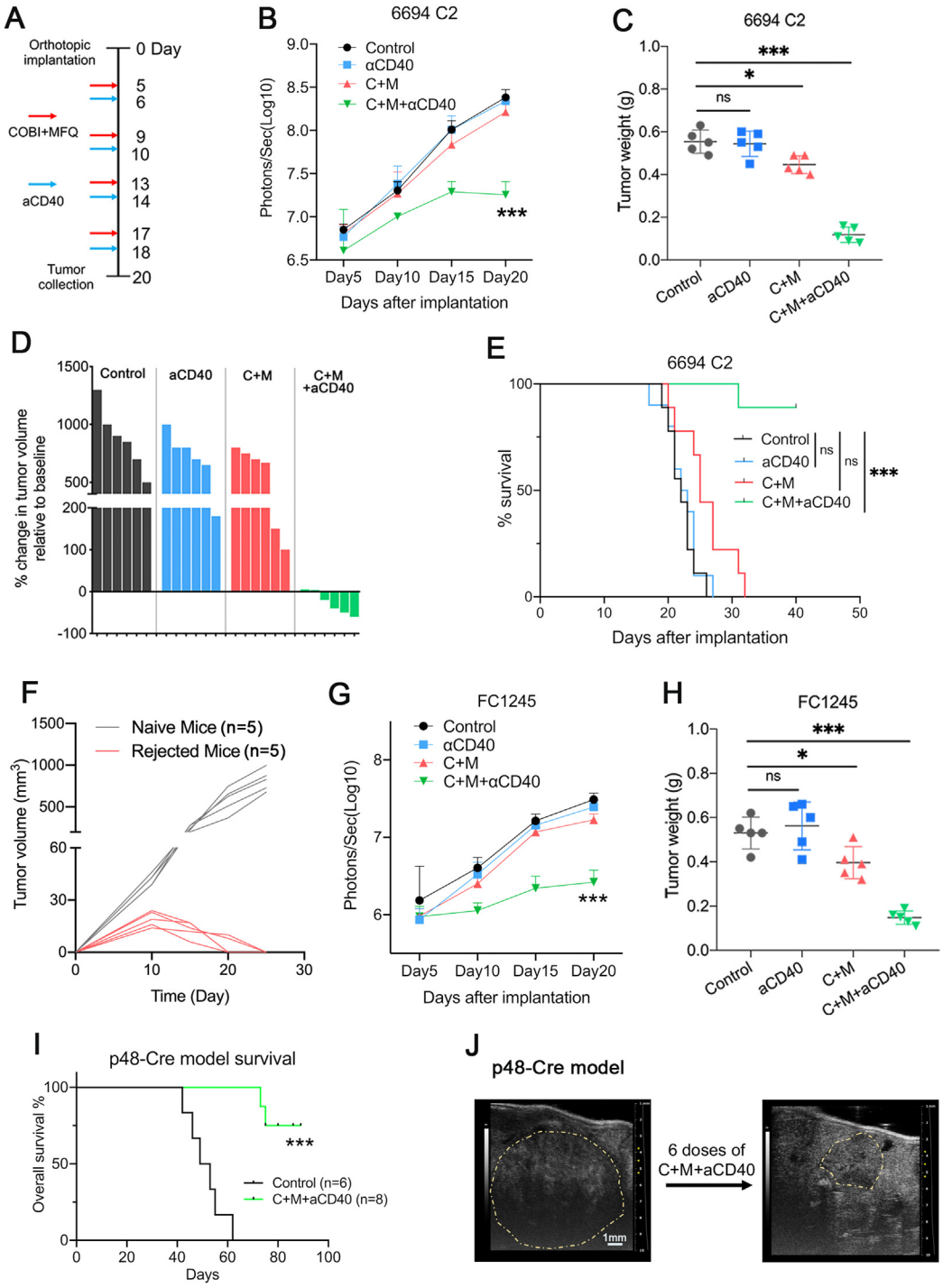

Figure 3. (*A*) Dosing schedule following C57BL/6J mice orthotopically implanted with mouse PDA cells. (*B*) Mean tumor growth and (*C*) tumor weights for mice bearing 6694C2-fLuc tumors with indicated treatments for 15 days. n = 5 mice/group. (*D*) Change in 6694C2 (non-fLuc labeled) tumor volume on day 25 compared with the start of treatment on day 10, representative of 6 mice per group. (*E*) Kaplan-Meier survival curves of mice engrafted with 6694C2 (non-fLuc labeled) tumors with indicated treatment for up to 40 days. Minimum n = 8 mice per group. (*F*) Tumor volume for mice after second subcutaneous injection of 6694C2 cells >40 days after being cured from the primary orthotopic implantation. Treatment-naïve WT C57BL/6J mice receiving first time subcutaneous injection challenge served as positive controls for tumorigenic capacity. (*G*) Mean tumor growth and (*H*) tumor weights for mice bearing FC1245-fLuc tumors with indicated treatments for 15 days. n = 5 mice/group. (*I*) Kaplan-Meier survival curves of KPC mice with indicated treatment for up to 90 days. n = 6 in control group and n = 8 in COBI/MFQ/aCD40 treatment group. (*J*) Representative ultrasound images reflecting change in KPC tumor volume after 6 doses of COBI + MFQ + aCD40 treatment. For (*B*–*H*), data reflect means ± SEMs, and 1 of 2 representative experiments. Significance was determined using a 2-way ANOVA (*B*, *G*), 1-way ANOVA (*C*, *H*), or log-rank test (*E*, *I*) and is shown as $^{*}P < .05$ and $^{***}P < .001$.

COBI/MFQ/aCD40 regimen further augmented this effect (Figure 4*E*). aCD40 alone or the triplet of COBI/MFQ/aCD40 strongly increased effector memory CD4 Teff presence in the tumor while reducing Tregs and exhausting CD8 T-cell levels (Supplementary Figure 3*E*). COBI/MFQ/aCD40 also resulted in the increased presence of effector memory CD8 T

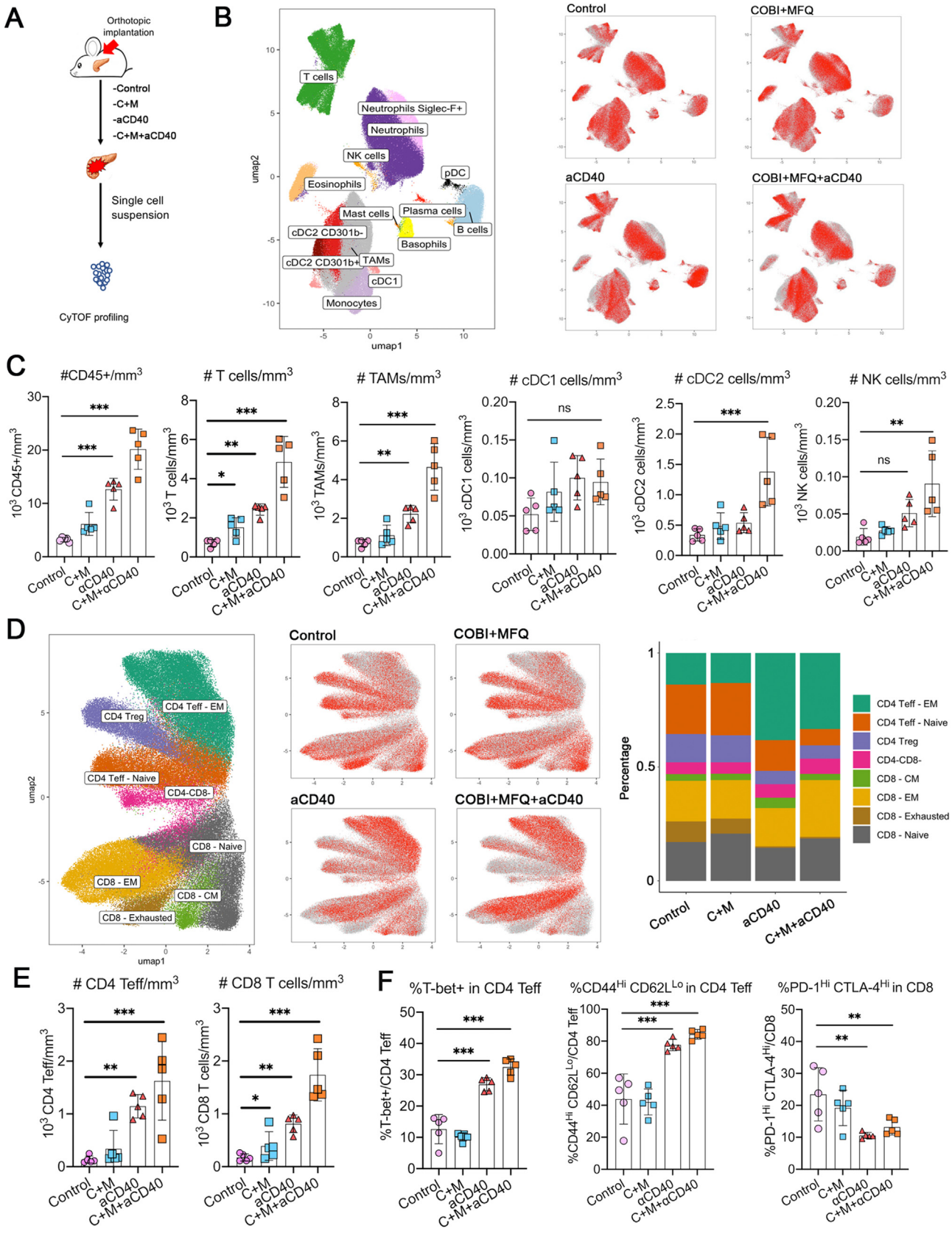

cells (Supplementary Figure 3*E*). We confirmed these phenotypic observations by manual gating and found a significant increase in T-bet$^+$ and CD44$^+$ CD62L$^-$ CD4 Teff cells and a striking decrease in PD-1$^+$ and CTL-4$^+$ CD8 T cells in COBI/MFQ/aCD40–treated tumors, supporting the presence of immune memory observed in the in vivo studies (Figure 4*F*).

In the p48-cre KPC model, both flow cytometry and histologic analyses revealed a remarkable increase in the infiltration of CD4$^+$ and CD8$^+$ T cells and higher Ki67+ frequency in CD8$^+$ T cells in COBI/MFQ/aCD40–treated tumors (Supplementary Figure 4*A*–*B*).

Given the increased infiltration of CD8$^+$ T cells on treatment, we investigated whether PD-L1 checkpoint inhibitor could enhance tumor growth inhibition but observed that mice treated with COBI/MFQ/aCD40/anti-PD-L1 showed similar response rates as mice with COBI/MFQ/aCD40 (Supplementary Figure 5*A*). The addition of anti-PD-L1 treatment did not further enhance the CD8$^+$ T-cell infiltrates (Supplementary Figure 5*B*). The depletion of CD4$^+$ and CD8$^+$ T cells with anti-CD4 and anti-CD8 neutralizing antibody treatments administered before the initial treatment with COBI/MFQ/aCD40 demonstrated that both CD4$^+$ and CD8$^+$ T cells were required for the in vivo efficacy (Supplementary Figure 6*A* and *B*). As cancer-associated fibroblasts (CAFs) play a vital role in the PDA immune microenvironment, we next sought to analyze the effects of COBI/MFQ/aCD40 treatment on the populations of CAFs. We observed no difference on the percentage of fibroblasts in the tumors with different treatments (Supplementary Figure 5*C*). With flow cytometric analysis of several surface markers that distinguish the subset of inflammatory cancer associated fibroblasts (iCAFs), we observed no significant difference in the percentage of anti-alpha smooth muscle actin (αSMA)^{low} interleukin 6^{high} iCAFs in the tumors with different treatments (Supplementary Figure 5*C*). Taken together, our data reveals that a durable antitumor immunologic program is activated on the triple therapy in mice bearing "cold" PDA tumors.

Triplet of COBI/MFQ/aCD40 Promotes Immunogenic Macrophage Polarization

Because autophagy and MEK coinhibition with aCD40 increased the density of TAMs (Figure 4*C*), we next examined these macrophage treatment-induced phenotypes. First, we observed that macrophage expression of MHCII, a key component of the antitumorigenic M1-like phenotype, increased slightly with COBI/MFQ treatment and further with the aCD40 mono-treatment or the triplet of COBI/MFQ/aCD40 treatment. COBI/MFQ/aCD40 therapy also reduced the frequency of CD206^{Hi}MHCII^{LO} in TAMs, considered a part of the M2-like phenotype (Figure 5*A*). Moreover, COBI/MFQ/aCD40 treatment resulted in up-regulated transcription of macrophage M1 polarization genes (*Cxcl10*, *Tnfa*, *Il15*, *Nos2*), whereas M2-associated transcripts were down-regulated consistent with our CyTOF results (*Il10*, *Mrc1*, *Ym1*; Supplementary Figure 5*D*).

We next performed multiplexed immunofluorescence imaging (ie, CODEX)[28] to better characterize the intratumoral architecture at a single-cell and cellular interaction level. MHCII and CD206 expression tightly colocalized on macrophages, and T cells were often excluded along these boundaries in untreated tumors. In contrast, most of MHCII expression did not colocalize with CD206 in the treated tumors. T cells were also more homogenously infiltrated throughout the tumor area (Figure 5*C* and *D*). The overall infiltration of CD8$^+$ T cells, CD4$^+$ T cells, and MHCII$^+$ macrophages, which normalized to pan-CK$^+$ tumor cells, were all increased (Supplementary Figure 5*E*). Furthermore, pairwise cell-cell interactions between CD4$^+$ or CD8$^+$ T cells with MHCII$^+$ macrophages in COBI/MFQ/aCD40–treated tumors increased compared with untreated tumors, suggesting that COBI/MFQ/aCD40 treatment triggered enhanced antigen presentation with functionally important intercellular/microenvironmental sequelae (Figure 5*B*).

To demonstrate the communication between adenocarcinoma cells and macrophages, we next performed conditioned media transfer experiments in vitro. We first exposed primary isolated human macrophages to 5 days of macrophage colony-stimulating factor (M-CSF) to induce the M2 polarized state, and then exposed these M2 macrophages to media from 4 human PDA cell lines (MiaPaca2, HPAFII, Panc-02.03, and HPAC), which had been pretreated with COBI/MFQ for 72 hours, aCD40 alone, or the combination of the conditioned media with aCD40 (Figure 5*E*). The conditioned media + aCD40 in all cases increased macrophage activation, as evidenced by CD80 and CD86 up-regulation (Figure 5*F*). In contrast, direct treatment of macrophages with aCD40 or conditioned media had limited effect on macrophage repolarization in vitro (Figure 5*F*). Depletion of macrophages in vivo in the 6694C2 model through anti-F4/80 antibody depletion abrogated the response to COBI/MFQ/aCD40 treatment, indicating that the antitumor immunity in these settings is macrophage-dependent in addition to being CD8 T-cell–dependent (Supplementary Figure 6*A* and *B*). In

Figure 4. (*A*) Schematic illustration of orthotopic 6694C2 tumors'-infiltrating immune cells analysis using CyTOF. (*B*) Uniform manifold approximation and projection (UMAP) visualizations of immune populations (*left*) and individual groups overlays (*right*, *grey* = all immune cells, *red* = treatment group overlay) obtained after performing Phenograph unsupervised clustering of all CD45$^+$ cells extracted from the manual gating of each sample. (*C*) Density of CD45$^+$ cells, T cells, TAMs, cDC1, cDC2, and NK cells in orthotopic 6694C2 tumors with indicated treatments. n = 5 mice/group. (*D*) UMAP visualizations of T-cell subpopulations (*left*), individual groups overlays (*middle*, *grey* = all immune cells, *red* = treatment group overlay), and bar graph showing the mean frequency of each cluster per group (*right*) obtained after performing Phenograph unsupervised clustering of T cells extracted from the manual gating of each sample. (*E*) Density of total CD4$^+$ Teff cells and CD8$^+$ T cells, calculated using the populations shown in (*D*). n = 5 mice/group. (*F*) Frequency of T-bet$^+$, CD44^{Hi}CD62L^{Lo}in CD4$^+$ Teff cells, and PD-1^{Hi}CTLA-4^{Hi} in CD8$^+$ T cells, calculated using our manual gating strategy. n = 5 mice/group. For (*C*) and (*E*), data reflect means ± SEMs, and 1 of 2 representative experiments. Significance was determined using 1-way ANOVA and is shown as **P* < .05, ***P* < .01, and ****P* < .001.

addition, depletion of either $CD4^+$ or $CD8^+$ T cells had no effect on the macrophage polarization induced by COBI/MFQ/aCD40 treatment, suggesting that the repolarization of macrophages is largely independent of T cells (Supplementary Figure 6*C*). Together, these data suggest that the combined regimens of COBI/MFQ/aCD40 activated TAMs toward an

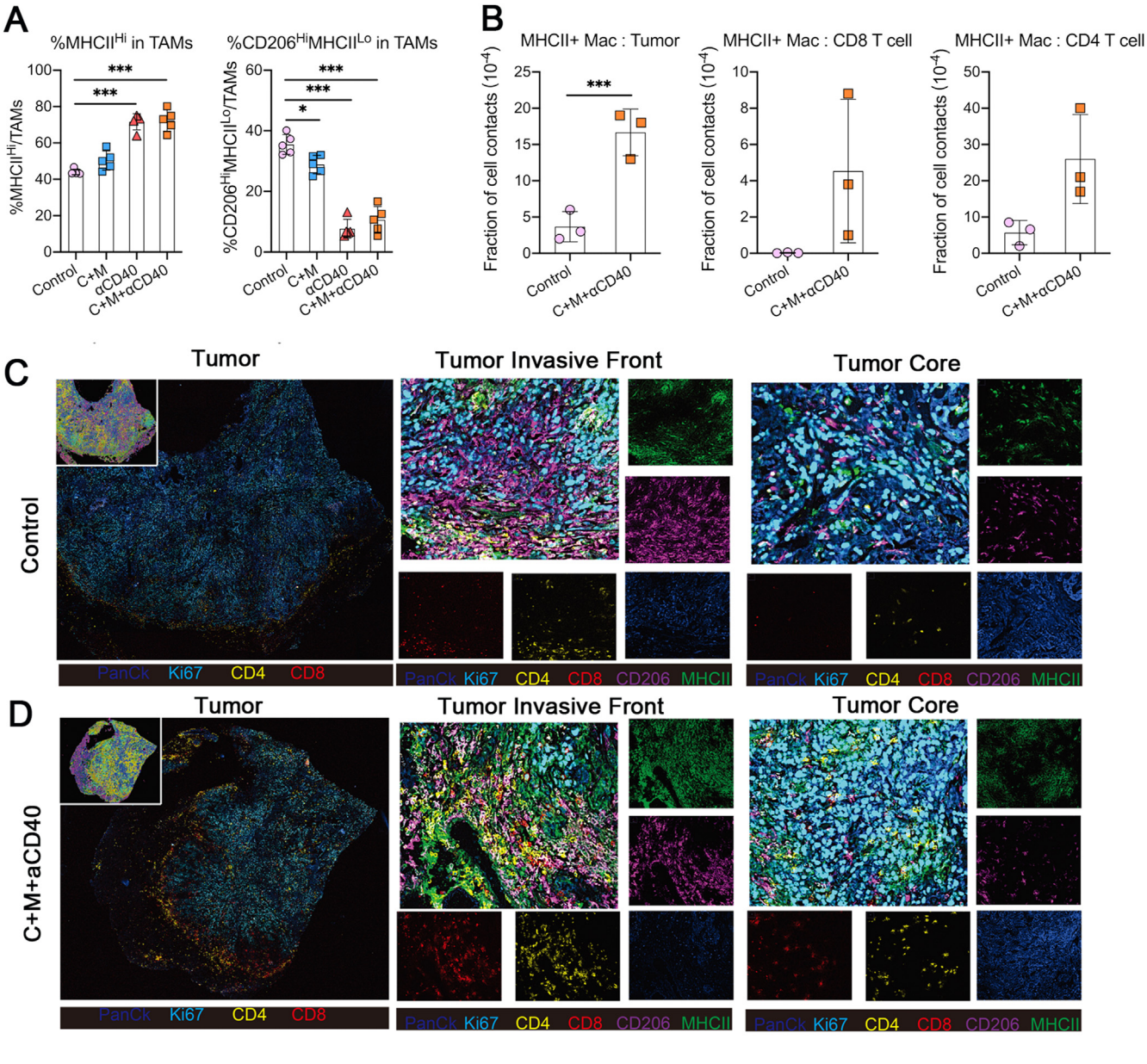

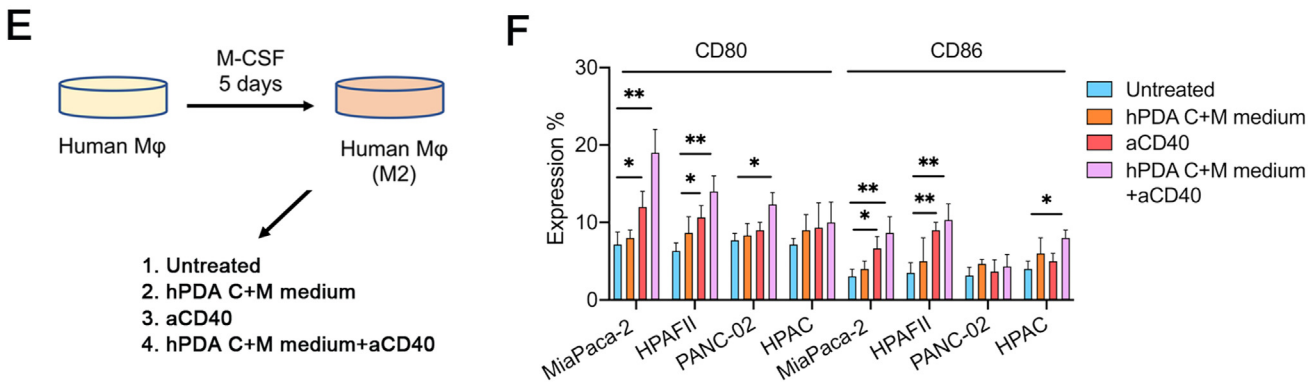

immunogenic M1-like phenotype through a paracrine mechanism involving PDA cells' production of diffusible signal(s), most likely type I IFNs.

CD40 Agonist Enhances COBI/MFQ Efficacy in a STING/Type I-IFN–Dependent Manner

STING is a critical driver of intracellular IFN transcriptional control.[29] To validate our hypothesis that the combination of COBI and MFQ synergizes with CD40 agonist was through STING activation, we administrated STING agonist (diABZI) alone or combined with aCD40 and observed similar tumor growth control compared with the triple therapy of COBI/MFQ/aCD40 (Figure 6*A*). The 6694C2 tumors receiving either diABZI alone or in combination with aCD40 exhibited a moderate increase in the $CD8^+$ T-cell infiltration (Figure 6*B*). However, the diABZI/aCD40 therapy was poorly tolerated over a continuous 15-day treatment (Supplementary Figure 6*D*). We next treated mice with type I IFN receptor blocking antibody in addition to COBI/MFQ/aCD40 to probe the requirement for type I IFNs in mediating COBI/MFQ/aCD40 efficacy. IFN depletion reversed triple therapy efficacy (Figure 6*C*). M1-like macrophages were also reduced after this blockade, which confirms that type I IFN are required for promoting immunogenic macrophage polarization (Figure 6*D*) and that this repolarization correlates with efficacy. Next, we aimed to quantify the extent to which the synergistic antitumor effect of combined COBI/MFQ/aCD40 therapy is mediated through tumor cell cyclic GMP–AMP synthase (cGAS)-STING activation. We depleted either cGAS or STING in 6694C2 cells using short hairpin RNA (shRNA) and verified knockdown efficiency using Western blot analysis (Figure 6*E*). Knockdown of cGAS or STING dramatically decreased tumor growth inhibition relative to sh-control–expressing tumors treated with the triplet regimen (Figure 6*F*, Supplementary Figure 6*E*), confirming the vital role of the cGAS/STING pathway in COBI/MFQ/aCD40–mediated antitumor response in a PDA model. We harvested treated tumors from this experiment for flow cytometry and observed that depletion of either STING or cGAS fully abrogated the macrophage M1 polarization (Figure 6*G*) and the infiltration of $CD8^+$ T cells (Figure 6*H*).

Discussion

Patients with PDA have not yet benefitted from immune checkpoint inhibition, largely due to the following: (1) a paucity of neoantigens arising from a relatively low tumor mutational burden, and (2) an immune-inhibitory microenvironment that dominantly antagonizes potentially tumoricidal T cells. In this study, we aimed to improve anticancer immunity in PDA, by focusing on RAS signaling in the PDA cancer cell itself. Using 2 mutant *Kras*-driven immunocompetent mouse models of PDA, we find that treatment with CD40 agonism combined with autophagy and MEK inhibition altered multiple immune subpopulations in the tumor immune microenvironment, transforming it from an immunosuppressive toward a T-cell–active milieu, and fostering durable immunologic control of tumor outgrowth. Combined blockade of autophagy and MEK activated the STING-type I-IFN pathway in PDA cells resulting in improved antigen presentation and subsequent robust infiltration of cytotoxic T cells mediated by M1-like TAMs.

Previous studies have highlighted autophagy's complex role in facilitating oncogenic RAS-driven proliferation. Lock et al[30] demonstrated that the autophagy pathway was required for efficient secretion of multiple cytokines, including interleukin 6, which promoted tumor cell invasion. Kinsey et al[31] and Bryant et al[5] also unveiled a protective role of autophagy in response to inhibition of RAS-RAF-ERK signaling to preserve tumor cell fitness in PDA. Yamamoto et al[32] then identified an autophagocytic processes as a driver of immuno-evasion in the tumor cell by the post-translational down-regulation of MHCI presentation and T-cell surveillance.

Successful therapeutic interventions must maximize efficacy and minimize toxicity. In the present study, we show that subcytotoxic doses of combined autophagy and MEK inhibitors triggered activation of the STING-type I IFN pathway in PDA cells. Encouragingly, the intermittent administration of COBI/MFQ (2 doses per week) plus aCD40 was sufficient for successful in vivo antitumor effects. Byrne et al[33] demonstrated that innate immune sensing pathways are not required for CD40 stimulation to trigger adaptive T-cell activation. We found that the primed STING-type I IFN signaling greatly boosted CD40-agonist–mediated antitumor immunity through a rigorous series of loss-of-function and depletion studies performed in vivo using relevant immunologically cold PDA systems closely reflecting the clinical disease in humans.

Pharmacologic aCD40 is being actively investigated in a variety of settings in oncology.[23,25,33,34] Single-agent aCD40 mAb modulated myeloid subpopulations in the tumor microenvironment in PDA, but it failed to achieve significant tumor control. Therefore, we examined the therapeutic

Figure 5. (*A*) Quantification of MHCII+ M1-like and CD206+MHCII- M2-like macrophage subsets among all TAMs, calculated using the manual gating strategy from Figure 4. (*B*) Quantification of cell-to-cell interaction scores between MHCII+ TAMs and tumor cells or CD8+ T cells or CD4+ T cells as determined using CODEX. Error bars represent mean ± SEM. (*C–D*) Representative multiplexed immunofluorescence images of COBI/MFQ/aCD40–treated and nontreated tumors determined using CODEX shows immune exclusion and immune infiltration. Zoom panel shows individual immune compartments, *blue* = anti-PanCK, *cyan* = anti-Ki67, *yellow* = anti-CD4, *red* = anti-CD8, *magenta* = anti-CD206, and *green* = anti-MHCII. (*E*) Schematic illustration of conditioned media transfer experiments in vitro. (*F*) Representative histogram assessing staining for CD80 (*left*) and CD86 (*right*) using flow cytometry in human macrophages treated with indicated drugs or conditioned media from a panel of human PDA cells. For (*A*), (*B*), and (*F*), data reflect means ± SEMs. Data in (*F*) is 1 of 2 representative experiments. Significance was determined using 1-way ANOVA and is shown as $^*P < .05$, $^{**}P < 0.01$, and $^{***}P < .001$.

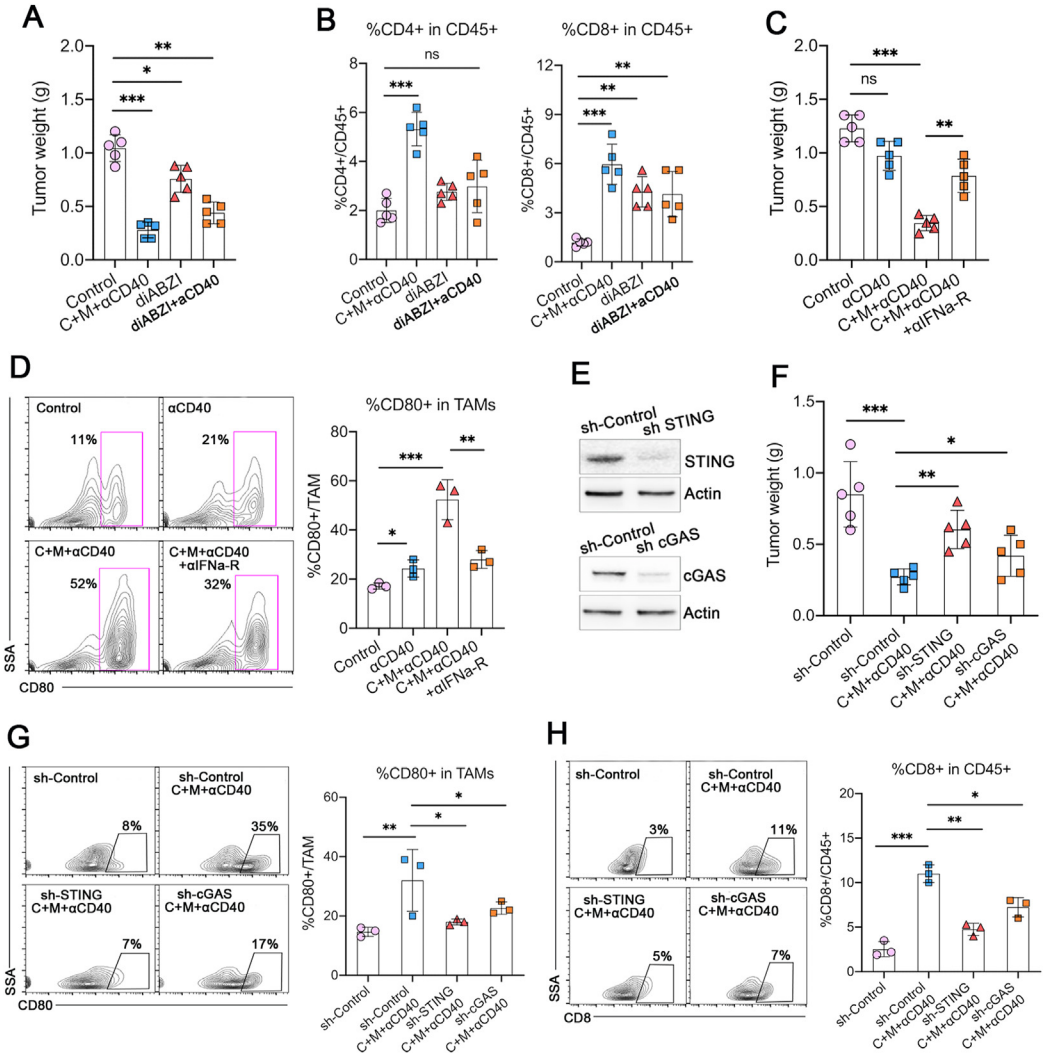

Figure 6. (*A*) Tumor weights of 6694C2-fLuc tumors with indicated treatments for 15 days. diABZI was administrated at 2 mg/kg every 4 days. N = 5 mice/group. (*B*) Quantification of $CD4^+$ and $CD8^+$ T cells among $CD45^+$ T cells in 6694C2-fLuc tumors with indicated treatments for 15 days. N = 5 mice/group. (*C*) Tumor weights of 6694C2-fLuc tumors with indicated treatments for 15 days. N = 5 mice/group. (*D*) Quantification of $CD80^+$ M1-like macrophage subsets out of $CD45^+$ cells in 6694C2 tumors with indicated treatment for 15 days. N = 3 mice/group. (*E*) Western blot for STING and cGAS in 6694C2 cells after indicated shRNA knockdown. (*F*) Tumor weights for mice bearing 6694C2-shCon tumor, 6694C2-sh-cGAS tumor, and 6694C2-sh-STING tumor with COBI/MFQ/aCD40 treatment for 15 days. N = 5mice/group. (*G*) Quantification of $CD80^+$ M1-like macrophage subsets out of $CD45^+$ cells in 6694C2-shCon tumor, 6694C2-sh-cGAS tumor, and 6694C2-sh-STING tumor with COBI/MFQ/aCD40 treatment for 15 days. N = 3mice/group. (*H*) Quantification of $CD8^+$ T cells out of $CD45^+$ cells in 6694C2-shCon tumor, 6694C2-sh-cGAS tumor, and 6694C2-sh-STING tumor with COBI/MFQ/aCD40 treatment for 15 days. N = 3 mice/group. For (*A–D*), (*F–H*), data reflect mean ± SEMs. Experiments were repeated once. Significance was determined using 1-way ANOVA and is shown as *P < .05, **P < .01, and ***P < .001.

benefits of aCD40 mAb as a partner with COBI/MFQ therapy in PDA models. We found that the triplet of COBI/MFQ/aCD40 therapy facilitated the shifting of TAMs toward an M1-like phenotype with concomitant T-cell infiltration to a much greater degree than aCD40 monotherapy. Furthermore, spatial distribution analysis using multiplexed immunofluorescence directly demonstrated increased cell-to-cell interaction frequencies between CD4 or CD8 T cells and MHCII–expressing TAMs, strongly supporting the hypothesis that enhanced antigen presenting is required in COBI/MFQ/aCD40–mediated antitumor immunity. Moreover, there appears to be additional activation of NK cells due to the triplet treatment, which is in agreement with previous findings[16] and warrants further investigation.

In summary, we show that MEK inhibition with concurrent autophagy blockade leads to a STING-dependent increase in type I IFN production from mouse and human *KRAS*-driven PDA cells. The activation of STING-type I IFN signaling can be augmented with therapeutic aCD40 to convert an immunologically exclusive tumor into one with effective T-cell infiltration. Our findings suggest that aCD40 may clinically synergize with MEK and autophagy inhibition to augment antitumor immunity in patients with PDA.

Supplementary Material

NOTE: To access the supplementary material accompanying this article, visit the online version of *Gastroenterology* at www.gastrojournal.org, and at http://doi.org/10.1053/j.gastro.2021.09.066.

References

1. Rahib L, Smith BD, Aizenberg R, et al. Projecting cancer incidence and deaths to 2030: the unexpected burden of thyroid, liver, and pancreas cancers in the United States. Cancer Res 2014;74. 2913–2321.
2. Ryan DP, Hong TS, Bardeesy N. Pancreatic adenocarcinoma. N Engl J Med 2014;371:1039–1049.
3. Almoguera C, Shibata D, Forrester K, et al. Most human carcinomas of the exocrine pancreas contain mutant c-K-ras genes. Cell 1988;53:549–554.
4. Collisson EA, Sadanandam A, Olson P, et al. Subtypes of pancreatic ductal adenocarcinoma and their differing responses to therapy. Nat Med 2011;17:500–503.
5. Bryant KL, Stalnecker CA, Zeitouni D, et al. Combination of ERK and autophagy inhibition as a treatment approach for pancreatic cancer. Nat Med 2019;25:628–640.
6. Kinsey CG, Camolotto SA, Boespflug AM, et al. Protective autophagy elicited by RAF–>MEK–>ERK inhibition suggests a treatment strategy for RAS-driven cancers. Nat Med 2019;25:620–627.
7. O'Reilly EM, Oh DY, Dhani N, et al. Durvalumab with or without Tremelimumab for patients with metastatic pancreatic ductal adenocarcinoma: a phase 2 randomized clinical trial. JAMA Oncol 2019;5:1431–1438.
8. Wainberg ZA, Hochster HS, Kim EJ, et al. Open-label, phase 1 study of Nivolumab combined with nab-Paclitaxel plus Gemcitabine in advanced pancreatic cancer. Clin Cancer Res 2020;26:4814–4822.
9. Marabelle A, Le DT, Ascierto PA, et al. Efficacy of Pembrolizumab in patients with noncolorectal high microsatellite instability/mismatch repair-deficient cancer: results from the phase II KEYNOTE-158 study. J Clin Oncol 2020;38:1–10.
10. Li J, Byrne KT, Yan F, et al. Tumor cell-intrinsic factors underlie heterogeneity of immune cell infiltration and response to immunotherapy. Immunity 2018;49:178–193.e7.
11. Allen BM, Hiam KJ, Burnett CE, et al. Systemic dysfunction and plasticity of the immune macroenvironment in cancer models. Nat Med 2020;26:1125–1134.
12. Levine JH, Simonds EF, Bendall SC, et al. Data-driven phenotypic dissection of AML reveals progenitor-like cells that correlate with prognosis. Cell 2015;162:184–197.
13. Sharma N, Thomas S, Golden EB, et al. Inhibition of autophagy and induction of breast cancer cell death by mefloquine, an antimalarial agent. Cancer Lett 2012;326:143–154.
14. Kimura S, Noda T, Yoshimori T. Dissection of the autophagosome maturation process by a novel reporter protein, tandem fluorescent-tagged LC3. Autophagy 2007;3:452–460.
15. Hou P, Kapoor A, Zhang Q, et al. Tumor Microenvironment Remodeling Enables Bypass of Oncogenic KRAS dependency in pancreatic cancer. Cancer Discov 2020;10:1058–1077.
16. Muthalagu N, Monteverde T, Raffo-Iraolagoitia X, et al. Repression of the type I interferon pathway underlies MYC- and KRAS-dependent evasion of NK and B Cells in pancreatic ductal adenocarcinoma. Cancer Discov 2020;10:872–887.
17. Wang MT, Fer N, Galeas J, et al. Blockade of leukemia inhibitory factor as a therapeutic approach to KRAS driven pancreatic cancer. Nat Commun 2019;10:3055.
18. Rees PA, Lowy RJ. Measuring type I interferon using reporter gene assays based on readily available cell lines. J Immunol Methods 2018;461:63–72.
19. Chou TC. Drug combination studies and their synergy quantification using the Chou-Talalay method. Cancer Res 2010;70:440–446.
20. Gessani S, Conti L, Del Corno M, et al. Type I interferons as regulators of human antigen presenting cell functions. Toxins (Basel) 2014;6:1696–1723.
21. Schiavoni G, Mattei F, Gabriele L. Type I interferons as stimulators of DC-mediated cross-priming: impact on anti-tumor response. Front Immunol 2013;4:483.
22. Hervas-Stubbs S, Perez-Gracia JL, Rouzaut A, et al. Direct effects of type I interferons on cells of the immune system. Clin Cancer Res 2011;17:2619–2627.
23. Beatty GL, Chiorean EG, Fishman MP, et al. CD40 agonists alter tumor stroma and show efficacy against pancreatic carcinoma in mice and humans. Science 2011;331:1612–1616.
24. Binnewies M, Mujal AM, Pollack JL, et al. Unleashing type-2 dendritic cells to drive protective antitumor CD4(+) T cell immunity. Cell 2019;177:556–571.e16.
25. Lin JH, Huffman AP, Wattenberg MM, et al. Type 1 conventional dendritic cells are systemically dysregulated early in pancreatic carcinogenesis. J Exp Med 2020;217:e20190673.
26. Pfirschke C, Engblom C, Gungabeesoon J, et al. Tumor-promoting Ly-6G(+) SiglecF(high) cells are mature and long-lived neutrophils. Cell Rep 2020;32:108164.
27. Marcus A, Mao AJ, Lensink-Vasan M, et al. Tumor-derived cGAMP triggers a STING-mediated interferon response in non-tumor cells to activate the NK cell response. Immunity 2018;49:754–763.e4.
28. Goltsev Y, Samusik N, Kennedy-Darling J, et al. Deep profiling of mouse splenic architecture with CODEX multiplexed imaging. Cell 2018;174:968–981.e15.
29. Barber GN. STING: infection, inflammation and cancer. Nat Rev Immunol 2015;15:760–770.
30. Lock R, Kenific CM, Leidal AM, et al. Autophagy-dependent production of secreted factors facilitates oncogenic RAS-driven invasion. Cancer Discov 2014;4:466–479.
31. Kinsey C, Camolotto SBA, Gullien K, et al. Protective autophagy elicited by RAF->MEK->ERK inhibition suggests a treatment strategy for RAS-driven cancers. Nature Med 2019;25:620–627.
32. Yamamoto K, Venida A, Yano J, et al. Autophagy promotes immune evasion of pancreatic cancer by degrading MHC-I. Nature 2020;581:100–105.

33. Byrne KT, Vonderheide RH. CD40 stimulation obviates innate sensors and drives T cell immunity in cancer. Cell Rep 2016;15:2719–2732.
34. Long KB, Gladney WL, Tooker GM, et al. IFNgamma and CCL2 cooperate to redirect tumor-infiltrating monocytes to degrade fibrosis and enhance chemotherapy efficacy in pancreatic carcinoma. Cancer Discov 2016;6:400–413.

Received February 19, 2021. Accepted September 30, 2021.

Correspondence
Address correspondence to: Eric A. Collisson, MD, Division of Hematology and Oncology, Department of Medicine, University of California, San Francisco, 1450 3rd Street, Room 375, San Francisco, California 94158. e-mail: collissonlab@gmail.com.

CRediT Authorship Contributions
Eric A. Collisson, MD (Conceptualization: Lead; Funding acquisition: Lead; Project administration: Lead; Supervision: Lead; Writing – original draft: Equal). Honglin Jiang, MD (Conceptualization: Lead; Data curation: Lead; Formal analysis: Lead; Investigation: Lead; Methodology: Lead; Writing – original draft: Lead). Tristan Courau, PhD (Data curation: Supporting; Methodology: Supporting). Joseph Borison, BS (Methodology: Supporting). Alexa J. Ritchie, BS (Methodology: Supporting). Aaron T. Mayer, PhD (Data curation: Supporting; Investigation: Supporting; Methodology: Supporting). Matthew F. Krummel, PhD (Project administration: Equal; Supervision: Equal).

Conflicts of interest
Eric A. Collisson is a consultant at Pear Diagnostics, IHP Therapeutics, and Valar Labs, reports receiving commercial research grants from Astra Zeneca, Merck KgA, and Bayer, and has stock ownership of Tatara Therapeutics, HDT Bio, Clara Health, BloodQ, and Guardant Health. The remaining authors disclose no conflicts.

Funding
This work was supported by the National Institutes of Health, National Cancer Institute Grants R01 (CA178015, CA222862, CA227807, CA239604, CA230263), U24 (CA210974), and U54 (CA224081) (E.A.C.). We ackowledge Dr Martin McMahon and Dr Ben Stanger for intellectual feedback and support. We also acknowledge the Preston, Sheresteia, and Rombauer families' support. Content does not reflect the views of the Department of Defense, American Cancer Society, National Cancer Institute, or National Institutes of Health.

Supplementary Materials and Methods

Animals and In Vivo Procedures

Treatment for tumor growth inhibition cohort was initiated on day 5 and for tumor regression cohort was initiated on day 10 after implantation with vehicle control (PBS/isotype control immunoglobulin G2a [IgG2a] mAb), aCD40 mAb (FKG45) at 100 μg intraperitoneal injection (ip) followed by COBI at 5 mg/kg (ip) and MFQ at 50 mg/kg (oral) every 4 days. In some experiments, CD8+ T cells, CD4+ T cells, or macrophages were depleted with each of clone 2.43, clone GK1.5, and clone CI:A3-1 neutralizing mAbs on day 4 after implantation and repeated every 4 days. Antibodies used were listed in Supplementary Table 1.

Single Tumor Cell Preparation

Single-cell suspensions of PDA tumors were prepared for CyTOF analysis as follows. Briefly, tumors were placed in cold RPMI-1640 medium with Collagenase IV (4 mg/mL) and DNase I (0.1 mg/mL), then minced to submillimeter pieces. Tissues were then incubated at 37℃ for 25 minutes with gentle shaking every 5 minutes. Specimens were filtered through a 70-mm mesh and centrifuged at 500*g* for 5 minutes at 4℃. Cells were then resuspend in RPMI-1640 medium with 2% serum for analysis.

Mass Cytometry (CyTOF)

We then manually gated the individual FCS files using FlowJo (BD, Ashland, OR) according to the gating scheme described in Supplementary Figure 7*A*. The antibodies used in our CyTOF panel are listed in Supplementary Table 2.

CODEX Multiplexed Imaging Analysis

Representation of the gating strategy was shown in Supplementary Figure 7*B*.

Cell Viability Assays

In this study, 3000–5000 cells optimized for each cell line were seeded on day 1, drugs were added on day 2 (using dimethyl sulfoxide normalized to 0.1%), and the cell viability was determined using CellTiter-Glo (Promega) on day 4. Viability curves were generated using GraphPad Prism 6.

Histologic Analysis

H&E staining and immunohistochemistry were performed on 4-μm–thick sections of 4% paraformaldehyde-fixed and paraffin-embedded tissues. Tail sections were decalcified using incubation of trimmed paraffin blocks for 10–15 minutes on paper towels soaked in 1 N HCl. Tumors sections were stained with anti-STING (13647), anti-STAT1 (14994), and anti-CD8a(14-0808-82).

B16 Cell–Mediated IFN Reporter Assay

B16-Blue cells (InvivoGen) were used to measure type I IFNs in collected media per the manufacturer's instructions. Briefly, cells were cultured in RPM-1640 medium containing 5% fetal bovine serum, 1% penicillin/streptomycin, and zeocin (100 μg/mL). Cells were then seeded at 50,000 cells per well in a 96-well plate. Conditioned media from FC1245 or 6694C2 cells with indicated treatment were added to B16 cells for 24 hours alongside IFNα (0–1000 U/mL) to generate a standard curve. QUANTI-Blue was then added in 1:1 vol/vol ratio for the following 24 hours. Media was transferred into a 96-well plate and measured using a plate reader.

Western Blotting

Tumor tissue and organ tissues was flash frozen in liquid nitrogen and homogenized in M-PER lysis buffer (Thermo Scientific) plus Halt protease and phosphatase inhibitor cocktail (Thermo Scientific). Protein concentrations were determined with the Pierce BCA Protein Assay Kit (Thermo Scientific), and extracts were loaded onto NuPAGE Bis–Tris SDS gels and immunoblots were visualized using the LiCOR Odyssey system. Antibodies used were listed in Supplementary Table 1.

Quantitative PCR Analysis for Gene Expression

RNA was prepared from cultured tumor cells or sorted cells from implanted tumors using RNeasy Mini Kit (QIAGEN). Complementary DNA was generated using High-capacity cDNA Reverse Transcription Kit (Bio-Rad). Quantitative PCR (qPCR) analysis was performed using TB Green Premix Ex Taq reagent (TaKaRa) and QuantStudio5 qPCR platform, and results were normalized to the expression of 18S ribosomal RNA. Primer sequences used for qPCR were listed in the Supplementary Table 1 on key resources.

In Vitro Synergy Assay

To evaluate synergy in vitro, cells were seeded into 96-well plates in complete medium, cultured overnight, and then treated in triplicate with COBI or MFQ, either alone or in various combinations. After 48 hours, cells were assayed using CellTiter-Glo (Promega) according to the manufacturer's protocol. Luminescence was quantified and analyzed with Combenefit software (Loewe model).

ELISA-Based IFN Determination

Supernatants from cells were collected at the indicated times. IFN-α and IFN-β were analyzed using ELISA kits (R&D Systems) with the manufacturer's instructions.

Lentivirus Transduction for shRNA-Mediated Knockdown

For stable and lentivirally transfected shRNA-based knockdown experiments, viruses were generated in HEK 293T cells transfected with lentiviral packaging vectors along with vectors expressing pGIPZ-shRNA using Fugene6

(Promega). Two distinct hairpins were chosen for the experiments. Tmem173(STING) shRNA (RMM4431-200316066) and Mb21d1(cGAS) shRNA (RMM4431-200322736) were purchased from Horizon Discovery. Viral supernatant collected from confluent monoculture was filtered and used to infect 6694C2 cells. A total of 0.5×10^6 cells was seeded in 1 well of a 6-well chamber and allowed to grow overnight. The following day, cells were incubated with a 1:2 mixture of growth medium and viral supernatant collected from HEK 293T cells. Polybrene was added at 8 μg/mL.

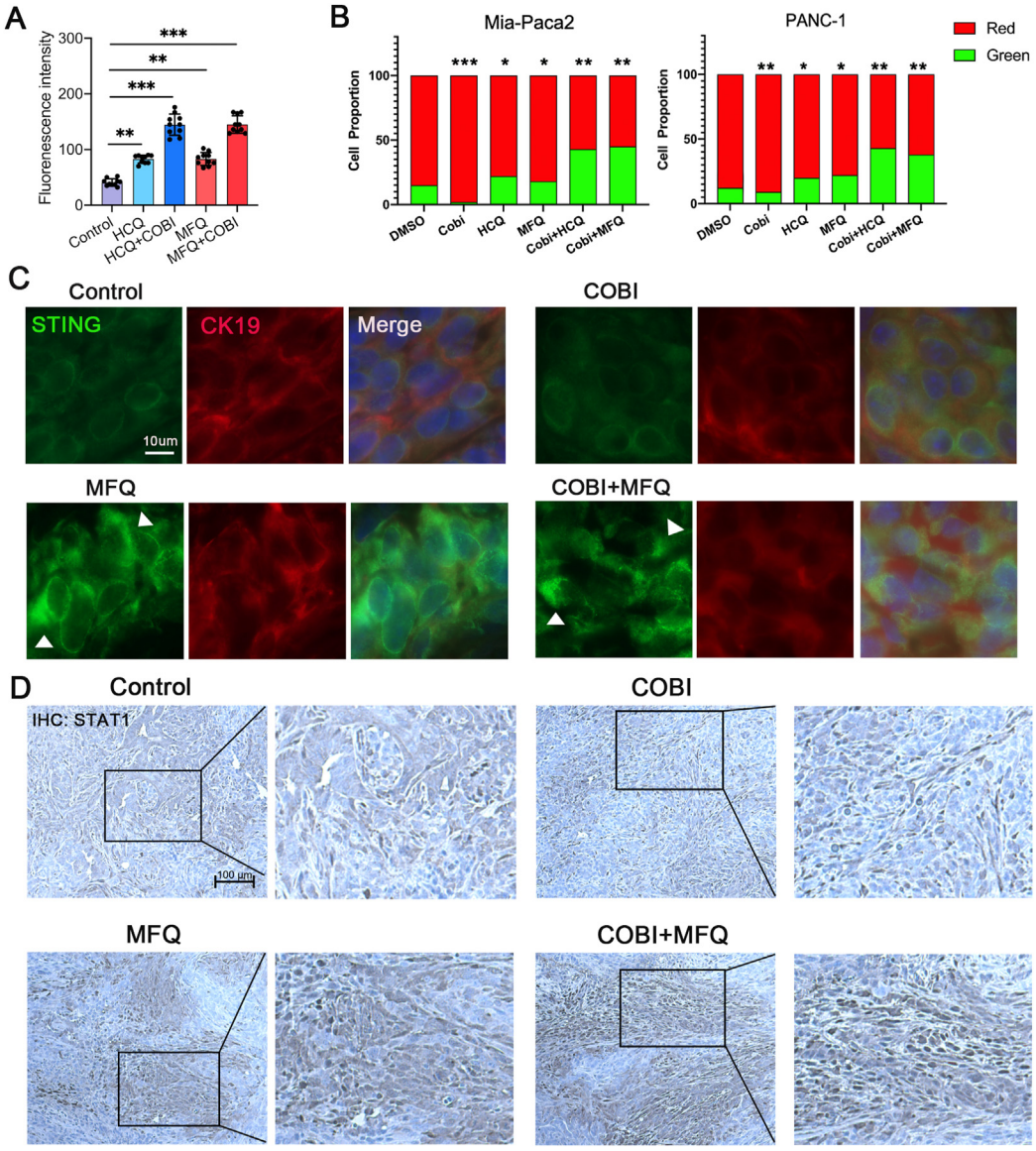

Supplementary Figure 1. (*A*) Quantification of fluorescence intensity for Figure 1*B*. 10–15 cells were analyzed in each treatment group. (*B*) Autophagic flux was assessed using flow cytometry in Mia-PaCa2 and PANC02 cells expressing mCherry-GFP-LC3AFR cells after 48 hours of indicated treatment. (*C*) Immunofluorescence analysis for STING and CK19 expression in 6694C2 tumors with indicated treatments for 20 days. Scale bars: 10 μm. (*D*) Immunohistochemistry of orthotopic 6694C2 tumors stained with STAT1 with indicated treatments for 20 days. Scale bars: 100 μm. For (*A*) and (*B*), data reflect means ± SEMs. All data is 1 of 2 representative experiments. Significance was determined using 1-way ANOVA and is shown as $^{*}P < .05$, $^{**}P < .01$, and $^{***}P < .001$.

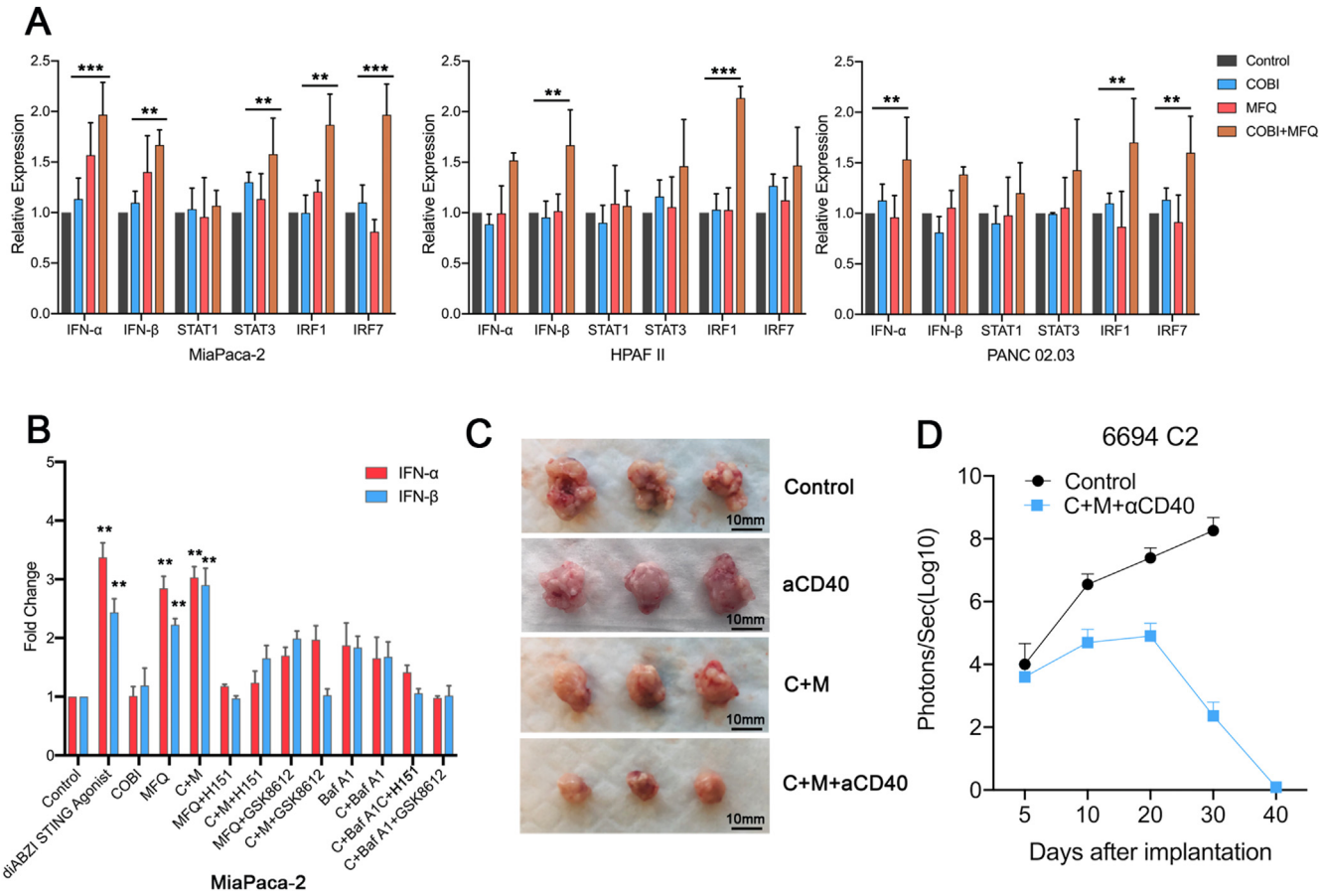

Supplementary Figure 2. (*A*) Quantitative polymerase chain reaction (PCR) analysis of IFN α/β, STAT1/3, and IRF1/7 in MiaPaca-2, HPAFII, and PANC02.03 cells with indicated treatment. (*B*) Enzyme-linked immunosorbent assay (ELISA) analysis for IFN-α/β production in MiaPaca-2 cells with indicated treatments for 18 hours. (*C*) Representative pictures of tumors for mice bearing 6694C2-fLuc tumors with indicated treatments for 15 days. Corresponding to Figure 3*B* and *C*. Scale bars: 10 mm. (*D*) Mean tumor growth for mice bearing 6694C2-fLuc tumors with indicated treatments for 40 days. N = 5 mice/group. For (*A*), (*B*), and (*D*), data reflect means ± SEMs. Data in (*A*) and (*B*) is 1 of 2 representative experiments. Significance was determined using 1-way ANOVA (*A*, *B*) and is shown as $^{*}P < .05$, $^{**}P < .01$, and $^{***}P < .001$.

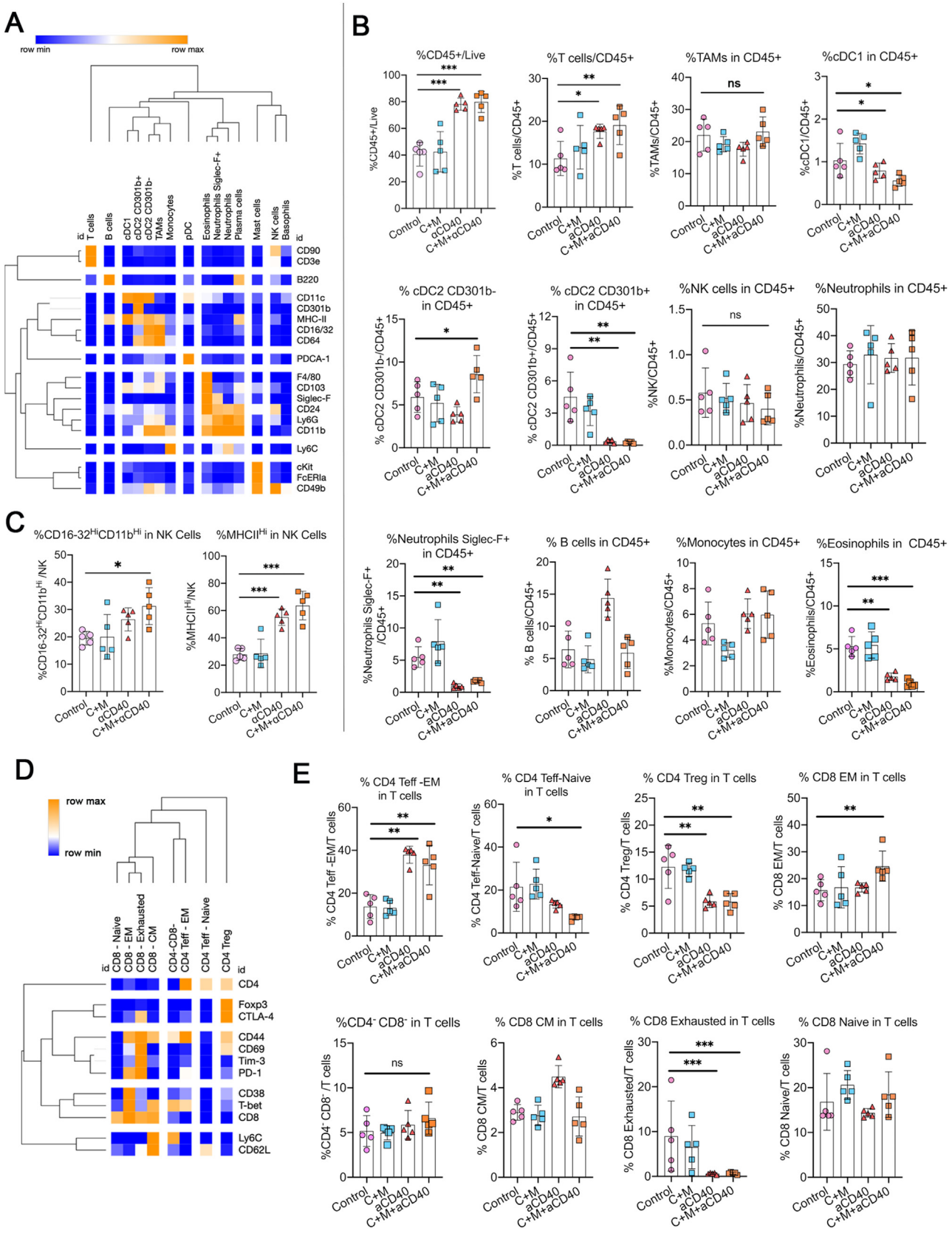
A
row min
row max
id
T cells
B cells
cDC1
cDC2 CD301b+
cDC2 CD301b-
TAMs
Monocytes
pDC
Eosinophils
Neutrophils Siglec-F+
Neutrophils
Plasma cells
Mast cells
NK cells
Basophils
CD90
CD3e
B220
CD11c
CD301b
MHC-II
CD16/32
CD64
PDCA-1
F4/80
CD103
Siglec-F
CD24
Ly6G
CD11b
Ly6C
cKit
FcERIa
CD49b
B
%CD45+/Live
%T cells/CD45+
%TAMs in CD45+
%cDC1 in CD45+
% cDC2 CD301b- in CD45+
% cDC2 CD301b+ in CD45+
%NK cells in CD45+
%Neutrophils in CD45+
%Neutrophils Siglec-F+ /CD45+
% B cells in CD45+
%Monocytes in CD45+
%Eosinophils in CD45+
Control
C+M
aCD40
C+M+aCD40
ns
C
%CD16-32HiCD11bHi in NK Cells
%MHCIIHi in NK Cells
D
row max
row min
CD8 - Naive
CD8 - EM
CD8 - Exhausted
CD8 - CM
CD4-CD8-
CD4 Teff - EM
CD4 Teff - Naive
CD4 Treg
CD4
Foxp3
CTLA-4
CD44
CD69
Tim-3
PD-1
CD38
T-bet
CD8
Ly6C
CD62L
E
% CD4 Teff -EM in T cells
% CD4 Teff-Naive in T cells
% CD4 Treg in T cells
% CD8 EM in T cells
%CD4- CD8- in T cells
% CD8 CM in T cells
% CD8 Exhausted in T cells
% CD8 Naive in T cells

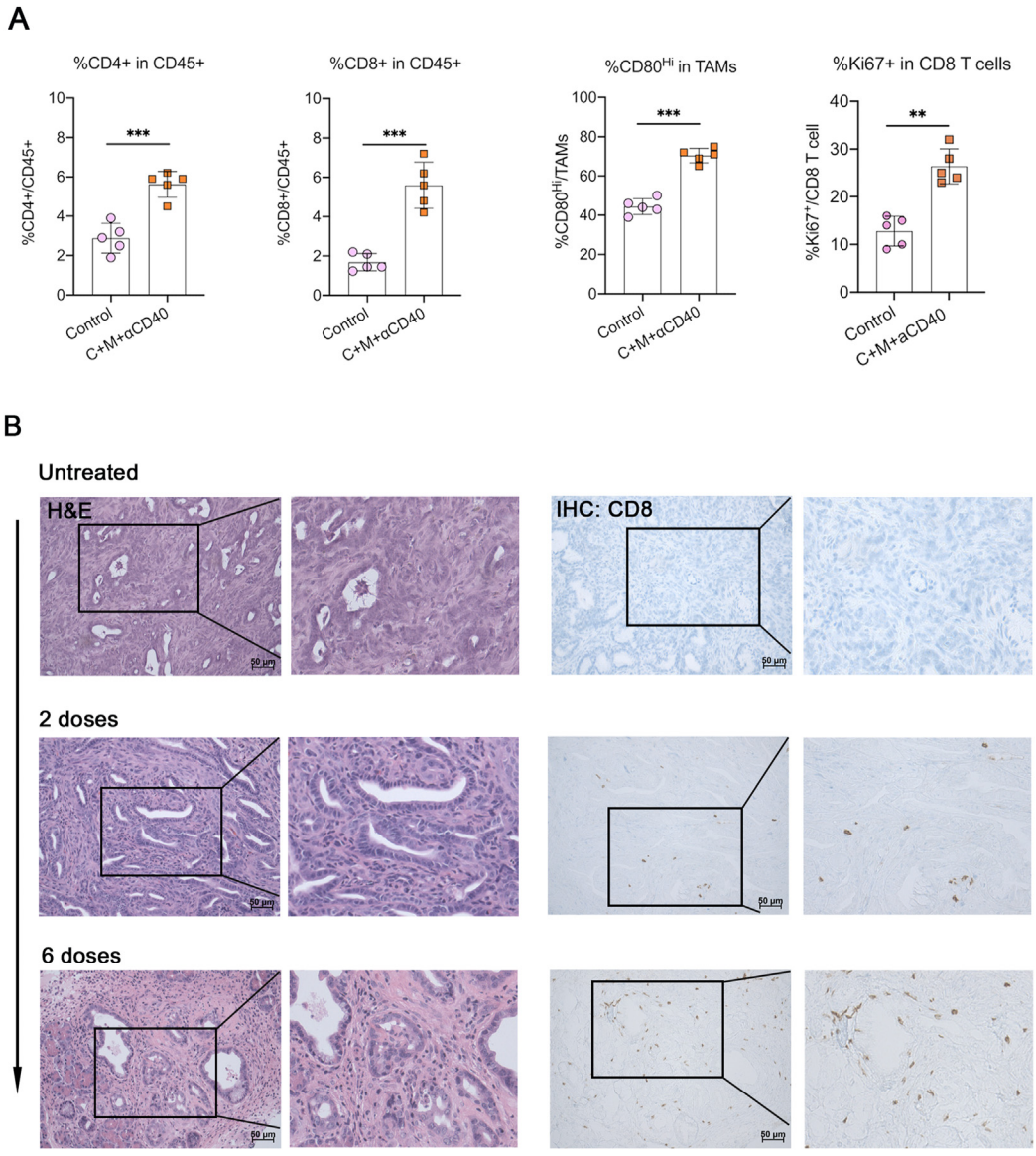

Supplementary Figure 4. (*A*) Quantification of $CD4^+$, $CD8^+$ T cells among $CD45^+$ cells, frequency of $CD80^{Hi}$ in TAMs and frequency of $Ki67^+$ in $CD8^+$ T cells in p48-cre KPC tumors with indicated treatments. (*B*) Images of H&E and immunohistochemistry staining with CD8 in p48-cre KPC tumors with indicated treatments. Scale bars: 50 μm. For (*A*), data reflect means ± SEMs. Data in (*C*) is 1 of 2 representative experiments. Significance was determined using *t* test (*A*) and is shown as $^*P < .05$, $^{**}P < .01$, and $^{***}P < .001$.

Supplementary Figure 3. Complementing results shown in Figure 4. (*A*) Heatmap showing median expression of lineage markers in the populations presented in Figure 4*B*. Both markers and clusters have undergone hierarchical clustering. (*B*) Quantification of immune populations frequencies presented in Figure 4*B*. n = 5 mice/group. (*C*) Frequency of $CD16/32^{Hi}CD11b^{Hi}$ and $MHCII^{Hi}$ in NK cells, calculated using our manual gating strategy. n = 5 mice/group. (*D*) Heatmap showing median expression of lineage and activation markers in the T-cell subpopulations presented in Figure 4*D*. Both markers and clusters have undergone hierarchical clustering. (*E*) Quantification of T-cell subpopulations frequencies presented in Figure 4*D*. n = 5 mice/group. For (*B*), (*C*), and (*E*), data reflect means ± SEMs, and 1 of 2 representative experiments. Significance was determined using 1-way ANOVA and is shown as $^*P < .05$, $^{**}P < .01$, and $^{***}P < .001$.

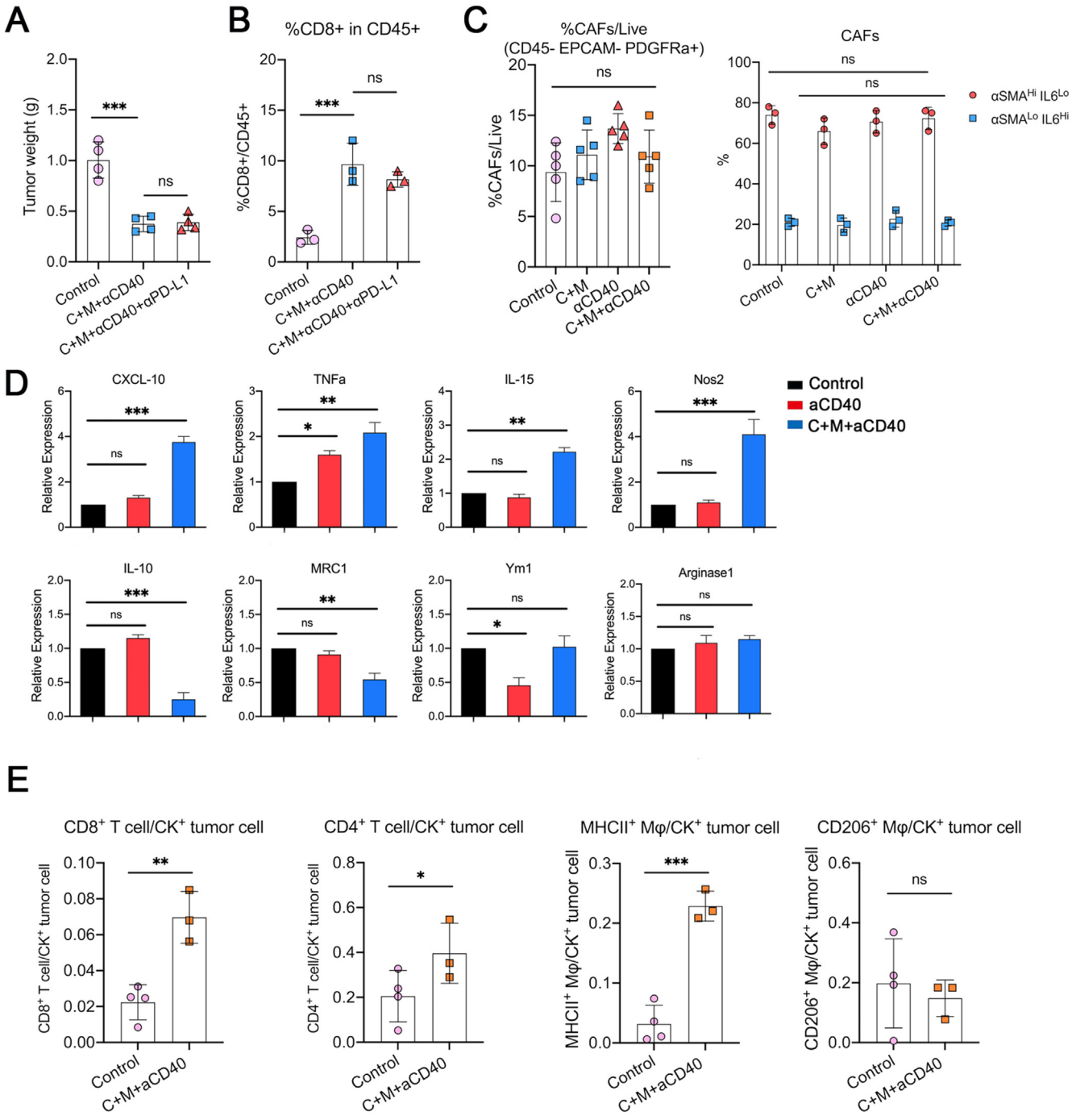

Supplementary Figure 5. (*A*) Tumor weights of tumors for mice bearing 6694C2-fLuc tumors with indicated treatments. N = 3–5 mice/group. (B) Quantification of $CD8^+$ T cells among $CD45^+$ cells in (*B*). N = 3–5 mice/group. (*C*) Flow cytometric analysis of CD45−EPCAM−PDGFRα+ fibroblasts in 6694C2 orthotopic tumors with indicated treatments, n = 5 mice/group. Flow cytometric analysis of anti-alpha smooth muscle actin (αSMA) and interleukin (IL) 6 in CAFs from 6694C2 orthotopic tumors with indicated treatments, n = 3 mice/group. (*D*) Quantitative PCR analysis of CXCL-10, tumor necrosis factor (TNF)α, IL15, NOS2, IL10, MRC1, YM1, and Arginase1 in macrophages freshly isolated from 6694C2 tumors with indicated treatments for 15 days. (*E*) Ratios of overall CD4+ T cells, $CD8^+$ T cells, $MHCII^+$ TAM, and CD206+ TAMs to $PanCK^+$ tumor cells in Figure 5*C* and *D*. N = 3–4 areas from 3 mice. For (*A–E*), data reflect means ± SEMs. Data in (*B*), (*C*), and (*D*) is 1 of 2 representative experiments. Significance was determined using 1-way ANOVA (*A–E*) and is shown as $^*P < .05$, $^{**}P < .01$, and $^{***}P < .001$.

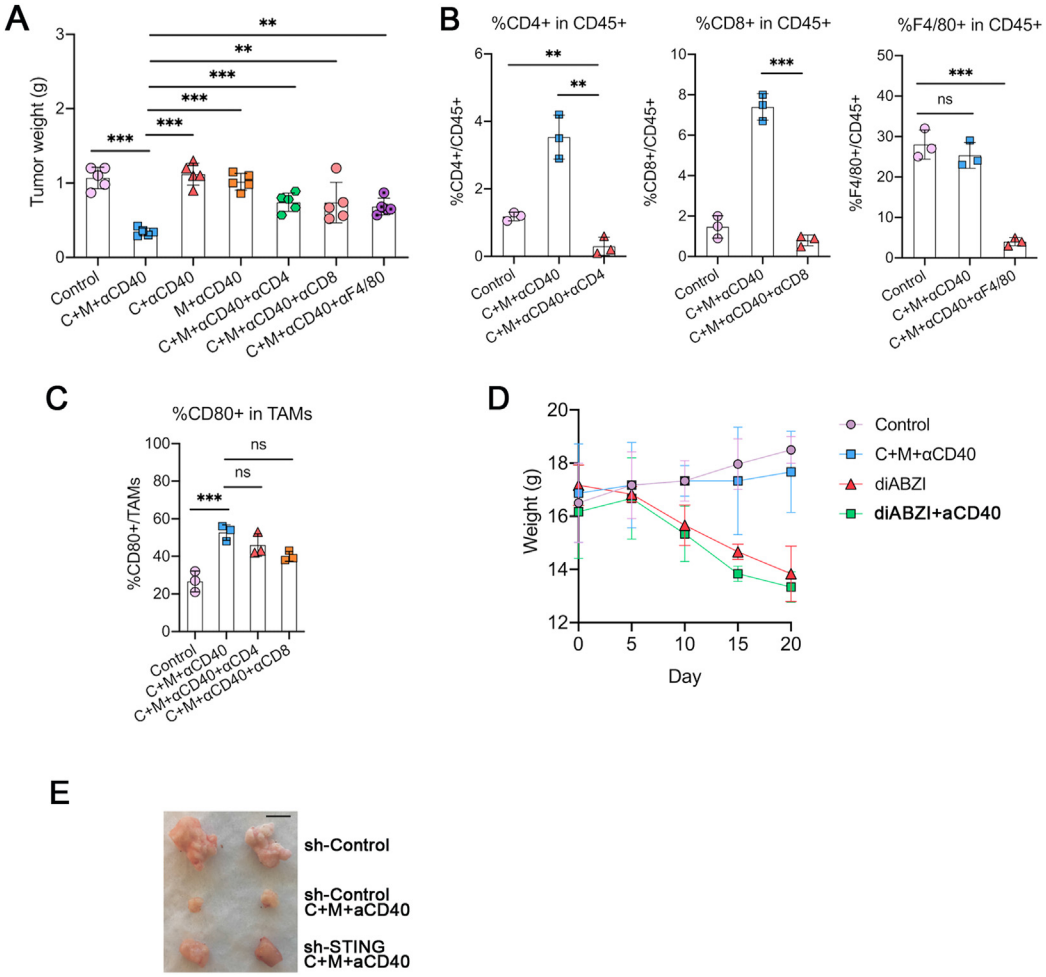

Supplementary Figure 6. (*A*) Tumor weights and representative pictures of tumors for mice bearing 6694C2-fLuc tumors with indicated treatments for 15 days. N = 5 mice/group. (*B*) Quantification depicting depletion of target cell type ($CD4^+$ T cell, $CD8^+$ T cell, and $F4/80^+$ TAMs) with antibody-based depletion treatment. N = 3 mice/group. (*C*) Frequency of $CD80^+$ in TAMs with indicated treatments for 15 days. N = 3 mice/group. (*D*) Mouse body weight changes with indicated treatments for 15 days. diABZI was administrated at the dose 2 mg/kg every 4 days. N = 5 mice/group. (*E*) Representative pictures of tumors for mice bearing 6694C2-shCon tumor, 6694C2-sh-cGAS tumor, and 6694C2-sh-STING tumor. Scale bars: 10 mm. For (*A–D*), data reflect means ± SEMs. Data in (*A*), (*B*), and (*C*) is 1 of 2 representative experiments. Significance was determined using 1-way ANOVA (*A–C*) and is shown as $^*P < .05$, $^{**}P < .01$, and $^{***}P < .001$.

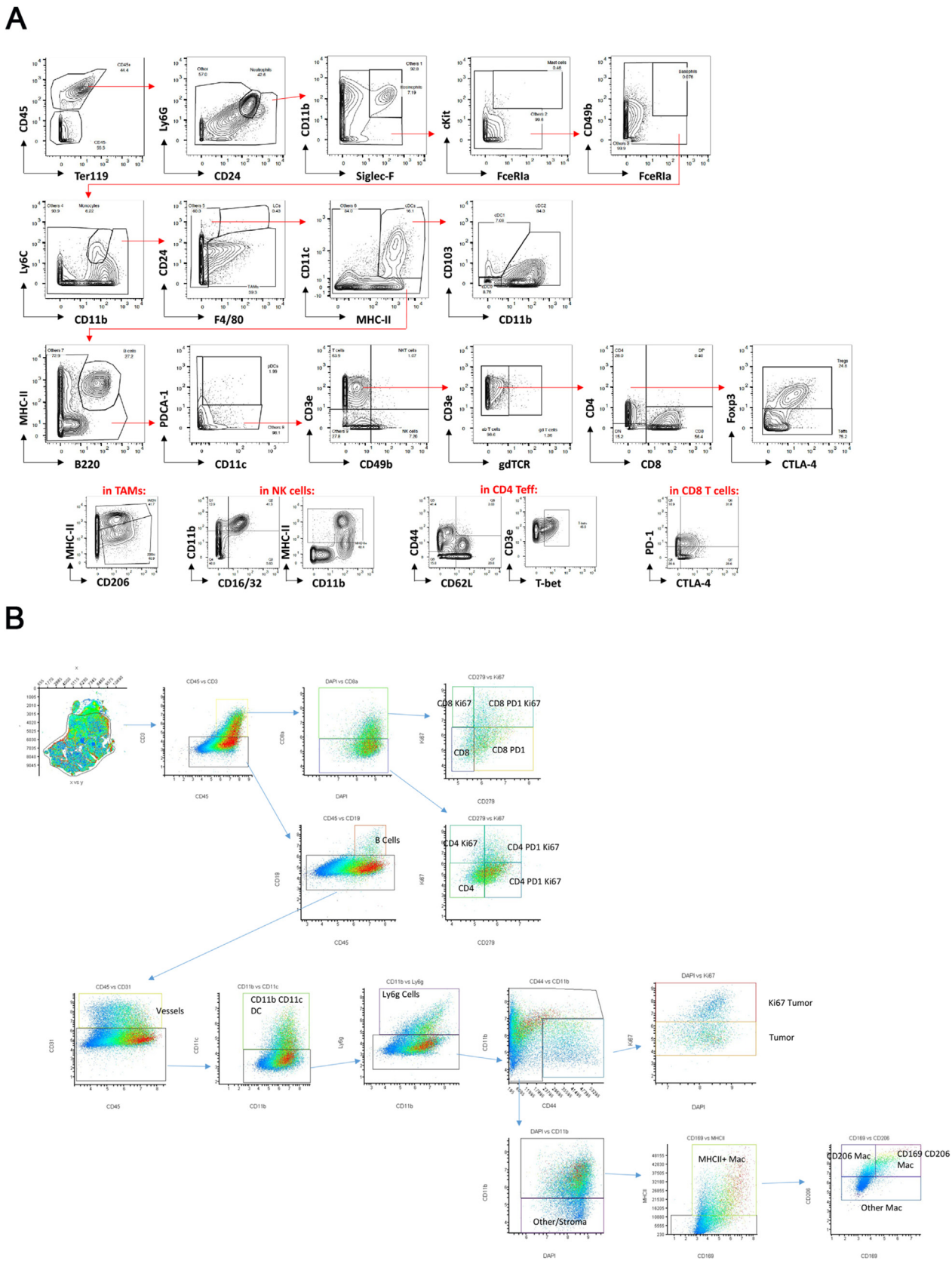

Supplementary Figure 7. (*A*) Representation of gating strategy used in CyTOF to identify various populations. (*B*) Representation of gating strategy used in CODEX multiplexed imaging analysis to identify various populations.

Supplementary Table 1. Key Resources

Reagent or resource	Source	Identifier
Antibodies		
WB: LC3B	Cell Signaling Technology	3868
WB: P62	Cell Signaling Technology	39749
WB: Phospho-Erk1/2 (Thr202/Tyr204)	Cell Signaling Technology	4370
WB: GAPDH	Cell Signaling Technology	5174
WB: Pho-IRF3 (Ser396)	Cell Signaling Technology	29047
WB: HSP90	Cell Signaling Technology	4874
WB: STING	Cell Signaling Technology	13647
WB: IRF3	Cell Signaling Technology	4302
WB: Pho-TBK1(Ser172)	Cell Signaling Technology	5483
WB: TBK1	Cell Signaling Technology	3504
IF: STING (Alexa Flour 488)	Abcam	ab198950
IF: Cytokeratin-19 (Alexa Flour 647)	Abcam	Ab192980
FC: APC anti-mouse CD8a	Biolegend	100712
FC: PE/Cy7 anti-mouse CD80	Biolegend	104733
FC: FITC anti-CD4 (RM4-4)	eBioscience	11-0043-82
FC: FITC anti-CD8 (H35-17.2)	eBioscience	11-0083-82
FC: Alexa Flour 700 anti-F4/80 (BM8)	eBioscience	56-4801-82
FC: Brilliant Violet 421 anti-mouse CD45	Biolegend	103133
FC: PE anti-human CD80	Biolegend	305207
FC: FITC anti-human CD86	Biolegend	374203
FC: Alexa Flour 488 anti-mouse CD326	Biolegend	118210
FC: APC anti-mouse CD140a	Biolegend	135907
FC: PE anti-mouse IL6	Biolegend	504503
FC: APC Cy7 anti-mouse αSMA	Abcore	12-0159-05
IHC: anti-CD8a	eBioscience	14-0808-82
IHC: anti-STING	Cell Signaling Technology	13647
IHC: anti-STAT1	Cell Signaling Technology	14994
Chemicals, peptides, and recombinant proteins		
In vivo MAb anti-mouse CD40 (FKG45)	BioXcell	BE0016-2
In vivo MAb anti-mouse PD-L1 (B7-H1)	BioXcell	BE0101
In vivo MAb anti-human CD40	BioXcell	BE0189
In vivo MAb anti-mouse F4/80 (CI:A3-1)	BioXcell	BE0206
In vivo MAb rat IgG2a isotype control	BioXcell	BP0089
In vivo MAb anti-mouse CD8α (2.43)	BioXcell	BE0061
In vivo MAb anti-mouse CD4 (GK1.5)	BioXcell	BE0003
MFQ	Selleckchem	S4420
COBI	MedChemExpress	HY-13064
HCQ	Selleckchem	12799

Supplementary Table 1. Continued

Reagent or resource	Source	Identifier
Human recombinant M-CSF	Stem cell	78057
GSK8612	Selleckchem	S8872
H-151	Selleckchem	S6652
diABZI	Selleckchem	S8796
BafA1	Sigma	19-148
Critical commercial assays		
Pierce BCA Protein Assay Kit	Thermo Scientific	23225
CellTiter-Glo Luminescent Cell Viability Assay	Promega	G7570
Mouse IFN-alpha ELISA Kit	R&D	42120-1
Mouse IFN-beta ELISA Kit	R&D	42400-1
Experimental models: cell lines		
MiaPaca-2	ATCC	CRL-1420
HPAF II	ATCC	CRL-1997
HPAC	ATCC	CRL-2119
Panc 02.03	ATCC	CRL-2553
Panc 10.05	ATCC	CRL-2547
Human peripheral blood macrophages	Stem cell	70042
Murine Type I IFNs Sensor Cell (B16-Blue)	InvivoGen	bb-ifnt1
FC1245	D. Tuveson	PMID 25259922
6694C2	B. Stanger	PMID 29958801
Experimental models: mouse strains		
Mouse C57BL/6J	The Jackson Laboratory	000664
P48^{Cre}; Kras$^{LSL-G12D/+}$; Trp53$^{flox/flox}$ (KPC)	M Hebrok	
Software and algorithms		
Graphpad Prism 8	GraphPad	https://graphpad.com
Combenefit	Combenefit	PMID 27153664
CyTOF mass cytometer	Fluidigm	Fluidigm
ImageJ	Fiji	Fiji
FlowJo	BD	BD
Xenogen IVIS	PerkinElmer	PerkinElmer
Vevo 2100 Ultrasound	FUJIFILM	FUJIFILM
Oligonucleotides		
GIPZ Lentiviral Mouse Tmem173 shRNA	Horizon Discovery	RMM4431-200316066
GIPZ Lentiviral Mouse Mb21d1 shRNA	Horizon Discovery	RMM4431-200322736
mIFN-α_F TGCCCAGCAGATCAAGAAGG	Elim Biopharm	
mIFN-α_R TCAGGGGAAATTCCTGCACC	Elim Biopharm	
mIFN-β_F CGTGGGAGATGTCCTCAACT	Elim Biopharm	

Supplementary Table 1. Continued

Reagent or resource	Source	Identifier
mIFN-β_R AGATCTCTGCTCGGACCACC	Elim Biopharm	
mIFN-γ_F AGGAACTGGCAAAAGGATGGT	Elim Biopharm	
mIFN-γ_R CCCAGATACAACCCCGCAAT	Elim Biopharm	
mTNF-α_F GGTCTGGGCCATAGAACTGA	Elim Biopharm	
mTNF-α_R GGTCTGGGCCATAGAACTGA	Elim Biopharm	
mIL17_F TCAAAGCTCAGCGTGTCCAA	Elim Biopharm	
mIL17_R TCTTCATTGCGGTGGAGAGTC	Elim Biopharm	
mCXCL10_F CCTATGGCCCTCATTCTCAC	Elim Biopharm	
mCXCL10_R CTCATCCTGCTGGGTCTGAG	Elim Biopharm	
mCCL5_F TGCAGTCGTGTTTGTCACTC	Elim Biopharm	
mCCL5_R ATGCCCATTTTCCCAGGACC	Elim Biopharm	
mHIF1α_F AGGATGAGTTCTGAACGTCGAAA	Elim Biopharm	
mHIF1α_R CTGTCTAGACCACCGGCATC	Elim Biopharm	
mIL15_F CTGCCATCCATCCAGAACTC	Elim Biopharm	
mIL15_R AGCACTGCCTCTTCATGGTC	Elim Biopharm	
mNos2_F GTCGATGTCACATGCAGCTT	Elim Biopharm	
mNos2_R GAAGAAAACCCCTTGTGCTG	Elim Biopharm	
mIL10_F AGACACCTTGGTCTTGGAGC	Elim Biopharm	
mIL10_R TTTGAATTCCCTGGGTGAGA	Elim Biopharm	
mMRC1_F GTGGATTGTCTTGTGGAGCA	Elim Biopharm	
mMRC1_R TTGTGGTGAGCTGAAAGGTG	Elim Biopharm	
mYm1_F TTTCTCCAGTGTAGCCATCCTT	Elim Biopharm	
mYm1_R AGGAGCAGGAATCATTGACG	Elim Biopharm	
mArginas1_F TTTTTCCAGCAGACCAGCTT	Elim Biopharm	

Supplementary Table 1. Continued

Reagent or resource	Source	Identifier
mArginas1_R AGAGATTATCGGAGCGCCTT	Elim Biopharm	
hIFN-α_F AACTCCCCTGATGAATGCGG	Elim Biopharm	
hIFN-α_R TAGCAGGGGTGAGAGTCTTTG	Elim Biopharm	
hIFN-β_F AGTAGGCGACACTGTTCGTG	Elim Biopharm	
hIFN-β_R AGCCTCCCATTCAATTGCCA	Elim Biopharm	

Abbreviations: APC, allophycocyanin; ELISA, enzyme-linked immunoassay; FC, flow cytometry; FITC, fluorescein; GAPDH, glyceraldehyde-3-phosphate dehydrogenase; IF, immunofluorescence; IG, immunoglobulin; IHC, immunohistochemistry; Mab, monoclonal antibody; M-CSF, macrophage colony-stimulating factor; PE, phycoerythrin; shRNA, short hairpin RNA.

Supplementary Table 2. Antibodies in CyTOF Panel

Specificity	Supplier	Reference	Clone
B220	Biolegend	103202	RA3-6B2
CCR7	Biolegend	120101	4B12
CD103	Biolegend	121402	2E7
CD11b	Biolegend	101202	M1/70
CD11c	Biolegend	117302	N418
CD16/32	BD	553142	2.4G2
CD206	Biolegend	141702	C068C2
CD24	Biolegend	101802	M1/69
CD3e	Biolegend	100202	17A2
CD301b	Biolegend	146802	URA-1
CD38	Biolegend	102702	90

Supplementary Table 2. Continued

Specificity	Supplier	Reference	Clone
CD4	Biolegend	100506	RM4-5
CD44	Biolegend	103002	IM7
CD45	Biolegend	103102	30-F11
CD49b	Biolegend	103513	HMa2
CD62L	R&D	MAB5761	MAB5761
CD64	Biolegend	139302	X54-5/7.1
CD69	R&D	AF2386	Polyclonal
CD8	Biolegend	100702	53-6.7
CD86	Biolegend	105002	GL-1
CD90	Biolegend	105202	G7
cKit	Biolegend	105802	2B8
CTLA-4	Biolegend	106302	UC10-4B9
F4/80	Biolegend	123102	BM8
FcER1a	Biolegend	134302	MAR-1
Foxp3	eBiosciences	14-4771-80	NRRF-30
GATA3	Biolegend	653802	16E10A23
ICOS	Biolegend	313502	C398.4A
Ki67	eBiosciences	14-5698-82	SolA15
Ly6C	Biolegend	128002	HK1.4
Ly6G	Biolegend	127602	1A8
MHCII	Biolegend	107602	M5/114.15.2
PD-1	Biolegend	135202	29F.1A12
PD-L1	Biolegend	124302	10F.9G2
PDCA-1	Biolegend	127002	927
RORgt	eBiosciences	14-6981-82	B2D
Siglec-H	Biolegend	129602	551
SIRPa	Biolegend	144002	P84
T-bet	Biolegend	644802	4B10
TCRgd	Biolegend	118101	GL3
Ter119	Biolegend	116202	Ter119
Tim-3	Biolegend	134002	B8.2C12